Statistical Analysis of Atom-Bond Connectivity related Descriptors and their Polynomials of some molecular structures of COVID-19 drugs

B. CHALUVARAJU[1], SHAIKH AMEER BASHA[2] AND VYSHNAVI D[3]
[1,2,3]Department of Mathematics, Bangalore University,
Janabharathi Campus, Bengaluru-560 056
Karnataka, INDIA
E-mail: {bchaluvaraju/shaikhameerbasha/vyshnavidevaragudi}@gmail.com

Abstract

The statistical analysis of the different versions of the Atom-Bond Connectivity (ABC) Descriptors (indices) are used to infer the drug molecular structures that are helpful for chemical and medical scientists to find out the chemical and biological characteristics of drugs. In this article, we compute and analyze the linear and non linear regression models of the different versions of ABC indices and their polynomials of some Molecular structures of COVID-19 drugs.

Keywords: Molecular graph; Molecular descriptor; ABC indices; ABC polynomials.

AMS(2020): 05C31, 05C90, 92E10, 94C15, 97M60.

1 Introduction

The world is amidst a COVID-19 pandemic. As health agencies cooperate on the response - following the pandemic, prompting on basic intercessions, appropriating fundamental clinical supplies to those in need they are hustling to create and send protected and compelling immunizations. Vaccines (Antibodies) save a great many lives every year. Immunizations work via preparing constantly the body's defense mechanism– the immune system – to perceive and fight the infections and microbes they target. After vaccination, if the body is subsequently presented to those infection causing germs, the body is promptly prepared to annihilate them, forestalling ailment [1–4]. The literature shows that a few antiviral drugs like favipiravir, ribavirin, remdesiver, theaflavin, chloroquine, hydroxychloroquine, lopinavir, ritonavir, Thalodomide, arbidol, histadine, and 2-phenoxyehanol are examined to restrain the infection and transmission of the 2019-nCoV in vitro and along these lines acquired the idealistic outcomes. In last quarter of 2020 Pfizer and Bharat Biotech started working on covid shield and covaxin respectively. These drugs have shown a positive impact on the recovery of Covid-19 affected patients clinically. The

ingredients of covid shield vaccine are L-Histidine, L-Histidine hydrochloride monohydrate, Magnesium chloride hexahydrate, Polycarbonate 80, Ethanol, Sucrose, Sodium chloride, Disodium edetate dihydrate and water for injection. The ingredients of covaxin are 64g of whole-virion inactivated SARS-CoV-2 antigen(Strain:NIV-2020-770) and the other inactive ingredients such as aluminium hydroxide gel(250mg), TLR 7/8 agonist(imida20-quinolinone) 15mg, 2-phenoxyethanol 2.5mg and phosphate buffer saline upto 0.5ml.

Recently, Chaluvaraju et al [5], has showed that different versions of ABC indices have a good correlation with EC50 and IC50 inhibitors.
Graph polynomials were first introduced by J.J. Sylvester in 1878, and further studied by J. Petersen. Graph polynomials were developed to study the structural information of molecular graphs. The degree and distance based polynomials provides the information about topological indices. In this article, different types of atom bond connectivity polynomials associated with atom bond connectivity indices have been discussed for the molecular graphs of the drugs.

Let $G = (V, E)$ be a simple connected graph with vertex set $V(G)$ and edge set $E(G)$. A molecular graph is a graph such that its vertices correspond to the atoms and the edges to the bonds. Then the chemical structure of the drug can be expressed by a molecular graph, which is a model used to describe a synthetic compound. The degree (or, valency) $d(u)$ of a vertex u is the number of vertices adjacent to u. For all further notions and terminologies, we refer to [6–9].
A molecular descriptor focuses on the numerical portrayal of a molecular structure as totally as conceivable Molecular connectivity indices are the most generally utilized molecular descriptors. These molecular meters, are known as graph invariants because of their definitions from the ideas of the graph theory and are more generally referred to as topological indices as they depict the topology of a molecule. Numerous such descriptors have been considered in theoretical chemistry and have found some applications, especially in QSPR/QSAR/QSTR research [10–24].

2 Different Versions of the ABC indices

A few graph invariants discovered applications are at present utilized in chemical sciences, pharmacology, environmental sciences. One of these is the atom bond connectivity index (or ABC index for short). $i^{th} ABC$ index of a molecular graph is given by

$$f(x_i, y_i) = \sum_{j=1}^{k} \sqrt{\frac{x_i + y_i - 2}{x_i y_i}}$$

If $i = 1$, then $f(x_1, y_1) = ABC_1(G)$, where $x_1 = d(u)$ is the degree of atom u and $y_1 = d(v)$ is the degree of atom v. For a connected graph G the atom-bond connectivity index is introduced by Estrada et. al., [25]. If $i = 2$, then

$f(x_2, y_2) = ABC_2(G)$, where $x_2 = n(u)$ is the number of vertices of G whose distance to the vertex u is smaller than the distance to the vertex v and $y_2 = n(v)$. Graovac and Ghorbani [26] defined the second atom bond connectivity index of G. If $i = 3$, then $f(x_3, y_3) = ABC_3(G)$, where $x_3 = m(u)$ is the number of edges of G whose distance to the vertex u is smaller than the distance to the vertex v and $y_3 = m(v)$. Farahani [27] introduced the third atom bond connectivity index. If $i = 4$, then $f(x_4, y_4) = ABC_4(G)$, where $x_4 = s(u)$ is the sum of the degrees of all neighbors of the vertex u in G and $y_5 = \epsilon(v)$ and $y_4 = s(v)$. Ghorbani [28] defined the fourth atom-connectivity index of (G). If $i = 5$, then $f(x_5, y_5) = ABC_5(G)$, where $x_5 = \epsilon(u)$ is the maximum distance between u and any other vertex of G and is known as the eccentricity of the vertex u. Farahani [29] introduced the fifth atom bond connectivity index in terms of the eccentricity of the vertex and it is also known as eccentric atom bond connectivity index of G. If $i = 6$, then $f(x_6, y_6) = ABC_6(G)$, where $x_6 = d_2(u)$ is the 2-distance of the vertex u in G is the number of 2-neighbors (i.e., $N_2(u) = \{v \in V : d(u, v) = 2\}$) of u in G and $y_6 = d_2(v)$. Kulli [30] introduced the sixth atom bond connectivity index (or, Leaf atom bond connectivity index).

The ABC polynomial of a graph is given by $ABC_i(G, x) = \sum_{j=1}^{k} x^{\sqrt{\frac{x_i+y_i-2}{x_i y_i}}}$.

3 Molecular structures and bond partitions

The chemical structures along with their molecular graphs are shown in the Figure 1 which includes $(G_1, G_2, G_3, G_4, G_5, G_6)$ and Figure 2 which includes $(G_7, G_8, G_9, G_{10}, G_{11}, G_{12})$. For more details, we refer to [2,3,5,17–20,23,24,52].

Favipiravir:
Favipiravir is a pyrazinecarboxamide derivative with activity against RNA viruses. Favipiravir is converted to the ribofuranosyltriphosphate derivative by host enzymes and selectively inhibits the influenza viral RNA-dependent RNA polymerase. Let G_1 be the molecular graph of Favipiravir (Figure 1). The molecular graph has 11 atoms (vertices) and 11 bonds (edges). For more detail, one can refer to [40–42]. its bond partitions are given as follows: The Bond partitions of G_1 for ABC_1 are given by $P_{(1,3)} = 4$, $P_{(2,2)} = 1$, $P_{(2,3)} = 4$, $P_{(3,3)} = 2$. The Bond partitions of G_1 for ABC_2 are given by $P_{(1,9)} = 4$, $P_{(2,7)} = 1$, $P_{(3,6)} = 6$. The Bond partitions of G_1 for ABC_3 are given by $P_{(1,10)} = 4$, $P_{(2,8)} = 1$, $P_{(3,6)} = 6$. The Bond partitions of G_1 for ABC_4 are given by $P_{(3,5)} = 3$, $P_{(3,6)} = 1$, $P_{(5,5)} = 2$, $P_{(5,6)} = 2$, $P_{(5,8)} = 1$, $P_{(6,8)} = 2$. The Bond partitions of G_1 for ABC_5 are given by $P_{(3,3)} = 1$, $P_{(3,4)} = 3$, $P_{(4,4)} = 1$, $P_{(4,5)} = 6$. The Bond partitions of G_1 for ABC_6 are given by $P_{(2,2)} = 3$, $P_{(2,3)} = 2$, $P_{(2,4)} = 1$, $P_{(2,5)} = 1$, $P_{(3,3)} = 2$, $P_{(3,5)} = 1$, $P_{(4,5)} = 1$.

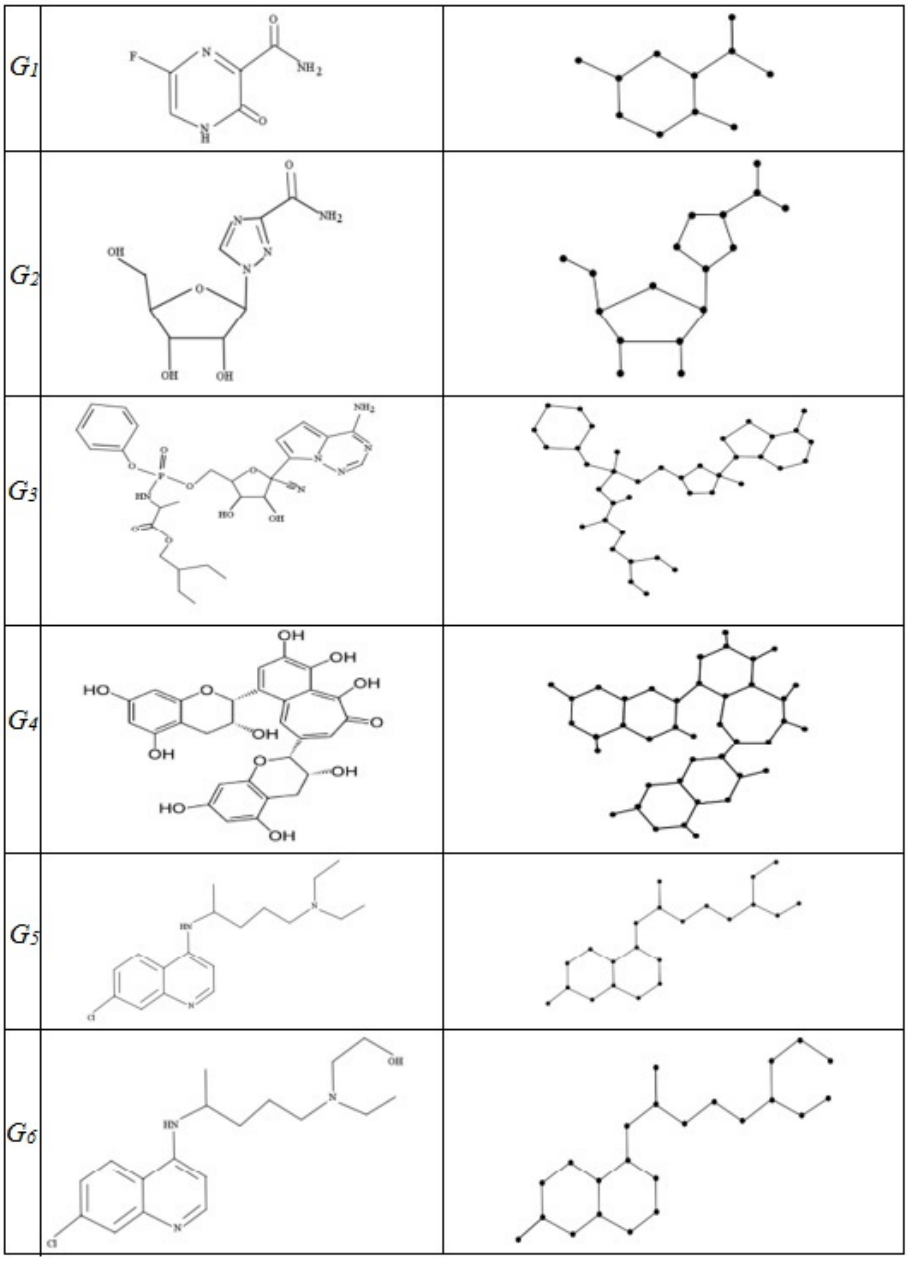

Figure 1: Chemical structures and their molecular graphs of $G_1, G_2, G_3, G_4, G_5, G_6$

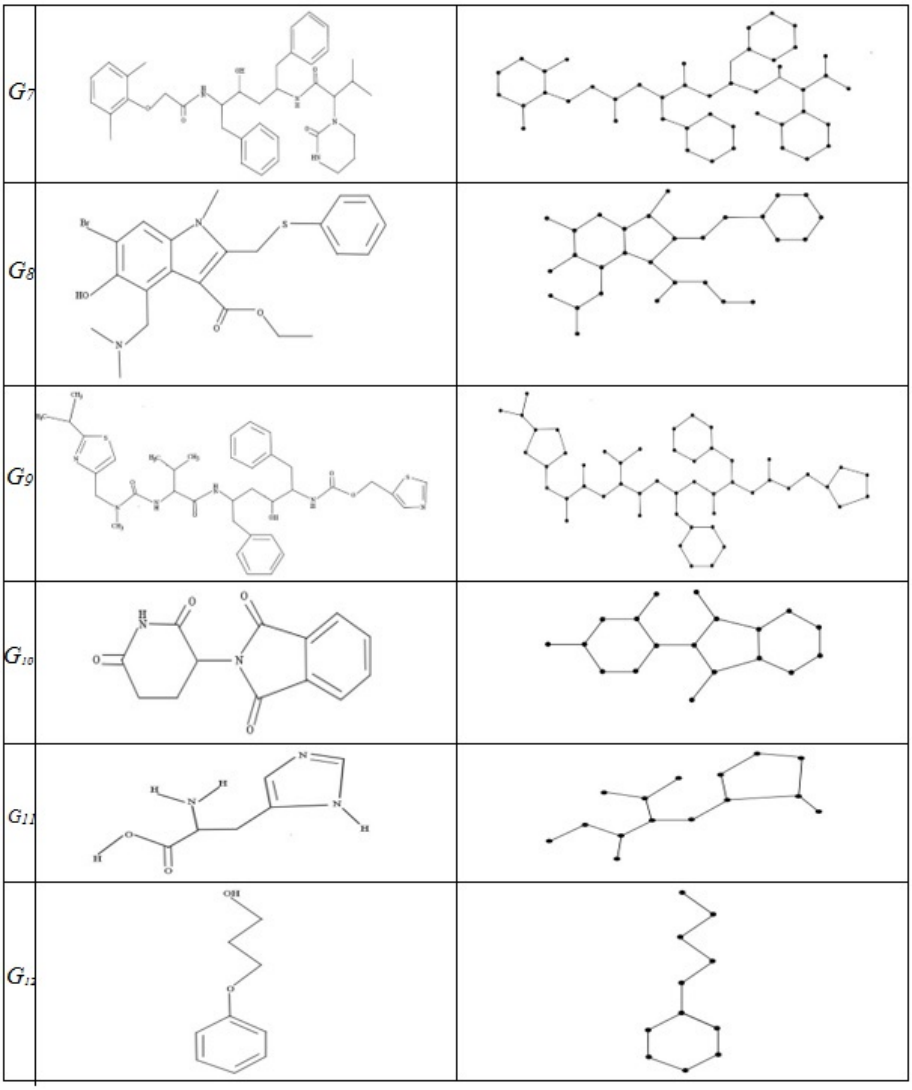

Figure 2: Chemicalstructures and their molecular graphs of $G_7, G_8, G_9, G_{10}, G_{11}, G_{12}$

Ribavirin:
Ribavirin is a nucleoside analogue and antiviral agent used in therapy of chronic hepatitis C and other flavivirus infections. Ribavirin has not been associated with clinically apparent liver injury. Let G_2 be the molecular graph of Ribavirin (Figure 1). The molecular graph has 17 atoms (vertices) and 18 bonds (edges). For more detail, see [43, 44].

The Bond partitions of G_2 for ABC_1 are given by $P_{(1,2)} = 1$, $P_{(1,3)} = 4$, $P_{(2,2)} = 1$, $P_{(2,3)} = 7$, $P_{(3,3)} = 5$. The Bond partitions of G_2 for ABC_2 are given by $P_{(1,4)} = 1$, $P_{(1,10)} = 1$, $P_{(1,14)} = 1$, $P_{(1,15)} = 5$, $P_{(2,3)} = 1$, $P_{(2,13)} = 1$, $P_{(3,9)} = 1$, $P_{(3,10)} = 1$, $P_{(4,9)} = 1$, $P_{(4,10)} = 3$, $P_{(4,11)} = 1$, $P_{(7,8)} = 1$. The Bond partitions of G_2 for ABC_3 are given by $P_{(1,16)} = 1$, $P_{(1,17)} = 5$, $P_{(2,5)} = 1$, $P_{(2,12)} = 1$, $P_{(2,15)} = 1$, $P_{(4,4)} = 1$, $P_{(4,11)} = 1$, $P_{(4,12)} = 1$, $P_{(5,11)} = 1$, $P_{(5,12)} = 4$, $P_{(8,9)} = 1$. The Bond partitions of G_2 for ABC_4 are given by $P_{(2,4)} = 1$, $P_{(3,5)} = 2$, $P_{(3,7)} = 2$, $P_{(4,7)} = 1$, $P_{(5,5)} = 1$, $P_{(5,7)} = 3$, $P_{(6,7)} = 3$, $P_{(6,8)} = 1$, $P_{(7,7)} = 2$, $P_{(7,8)} = 2$. The Bond partitions of G_2 for ABC_5 are given by $P_{(5,5)} = 1$, $P_{(5,6)} = 4$, $P_{(6,7)} = 6$, $P_{(7,7)} = 2$, $P_{(7,8)} = 3$, $P_{(8,9)} = 3$. The Bond partitions of G_2 for ABC_6 are given by $P_{(1,2)} = 1$, $P_{(2,2)} = 2$, $P_{(2,4)} = 4$, $P_{(3,3)} = 1$, $P_{(3,4)} = 2$, $P_{(4,4)} = 5$, $P_{(4,5)} = 3$.

Remdesivir:
Remdesivir is an antiviral nucleotide analogue used for therapy of severe novel coronavirus disease 2019 (COVID-19) caused by severe acute respiratory syndrome (SARS) coronavirus 2 (CoV-2) infection. Remdesivir therapy is given intravenously for 5 to 10 days and is frequently accompanied by transient, reversible mild-to-moderate elevations in serum aminotransferase levels but has been only rarely linked to instances of clinically apparent liver injury, its hepatic effects being overshadowed by the systemic effects of COVID-19. Let G_3 be the molecular graph of Remdesivir (Figure 1). The molecular graph has 41 atoms (vertices) and 44 bonds (edges). For more detail, see [45, 46].

The Bond partitions of G_3 for ABC_1 are given by $P_{(1,2)} = 2$, $P_{(1,3)} = 5$, $P_{(1,4)} = 2$,$P_{(2,2)} = 9$, $P_{(2,3)} = 14$, $P_{(2,4)} = 4$, $P_{(3,3)} = 6$, $P_{(3,4)} = 2$. The Bond partitions of G_3 for ABC_2 are given by $P_{(1,6)} = 1$, $P_{(1,34)} = 1$, $P_{(1,38)} = 2$, $P_{(1,39)} = 9$, $P_{(2,37)} = 8$, $P_{(3,12)} = 1$, $P_{(3,23)} = 1$, $P_{(3,36)} = 2$, $P_{(4,32)} = 1$, $P_{(4,33)} = 1$, $P_{(4,34)} = 1$, $P_{(4,35)} = 1$, $P_{(5,34)} = 2$, $P_{(6,32)} = 1$, $P_{(6,33)} = 2$, $P_{(8,31)} = 1$, $P_{(9,30)} = 1$, $P_{(10,29)} = 1$, $P_{(11,28)} = 1$, $P_{(12,24)} = 1$, $P_{(13,24)} = 1$, $P_{(13,25)} = 1$, $P_{(17,22)} = 1$, $P_{(18,21)} = 1$, $P_{(19,20)} = 1$. The Bond partitions of G_3 for ABC_3 are given by $P_{(1,42)} = 2$, $P_{(1,43)} = 9$, $P_{(2,8)} = 1$, $P_{(2,32)} = 1$, $P_{(2,40)} = 2$, $P_{(2,41)} = 6$, $P_{(3,39)} = 2$, $P_{(4,15)} = 1$, $P_{(4,26)} = 1$, $P_{(4,39)} = 1$, $P_{(5,37)} = 2$, $P_{(5,38)} = 1$, $P_{(6,35)} = 1$, $P_{(6,37)} = 2$, $P_{(7,36)} = 1$, $P_{(8,35)} = 2$, $P_{(10,33)} = 1$, $P_{(11,32)} = 2$, $P_{(15,27)} = 1$, $P_{(16,26)} = 1$, $P_{(16,27)} = 1$, $P_{(20,23)} = 1$, $P_{(21,22)} = 2$. The Bond partitions of G_3 for ABC_4 are given by $P_{(2,4)} = 2$, $P_{(3,6)} = 3$, $P_{(3,7)} = 1$, $P_{(3,8)} = 1$, $P_{(4,4)} = 2$, $P_{(4,5)} = 4$, $P_{(4,6)} = 2$, $P_{(4,7)} = 1$, $P_{(4,9)} = 1$, $P_{(5,5)} = 2$, $P_{(5,6)} = 6$, $P_{(5,7)} = 1$, $P_{(5,8)} = 2$, $P_{(5,9)} = 1$, $P_{(6,6)} = 1$, $P_{(6,7)} = 3$, $P_{(6,8)} = 1$, $P_{(7,7)} = 4$, $P_{(7,8)} = 1$, $P_{(7,9)} = 1$, $P_{(8,8)} = 1$, $P_{(8,9)} = 2$, $P_{(9,9)} = 1$. The Bond partitions of G_3 for ABC_5 are given by $P_{(9,10)} = 2$, $P_{(10,11)} = 4$, $P_{(11,12)} = 4$, $P_{(12,13)} = 7$, $P_{(13,13)} = 1$, $P_{(13,14)} = 7$, $P_{(14,15)} = 5$, $P_{(15,16)} = 4$, $P_{(16,16)} = 1$, $P_{(16,17)} = 4$, $P_{(17,18)} = 5$. The Bond partitions of G_3 for ABC_6 are given by $P_{(1,2)} = 2$, $P_{(2,2)} = 3$, $P_{(2,3)} = 10$, $P_{(2,4)} = 1$, $P_{(2,5)} = 1$, $P_{(3,3)} = 7$, $P_{(3,4)} = 3$, $P_{(3,5)} = 8$, $P_{(3,6)} = 1$, $P_{(4,4)} = 1$, $P_{(4,5)} = 2$, $P_{(5,5)} = 3$, $P_{(5,6)} = 2$.

Theaflavin:
Theaflavin is a biflavonoid that is 3,4,5-trihydroxybenzocyclohepten-6-one which is substituted at positions 1 and 8 by (2R,3R)-3,5,7-trihydroxy-3,4-dihydro-2H-chromen-2-yl groups. It is the main red pigment in black tea. It has a role as an antioxidant, a chelator, a plant metabolite, a radiation protective agent and an antibacterial agent. It is a polyphenol and a biflavonoid. G_4 be the molecular graph of Theaflavin (Figure 4). The molecular graph has 41 atoms (vertices) and 46 bonds (edges). For more detail, see [47, 48]. The Bond partitions of G_4 for ABC_1 are given by $P_{(1,3)} = 10$, $P_{(2,3)} = 22$, $P_{(3,3)} = 14$. The Bond partitions of G_4 for ABC_2 are given by $P_{(1,40)} = 10$, $P_{(3,36)} = 5$, $P_{(4,21)} = 1$, $P_{(4,30)} = 1$, $P_{(4,35)} = 6$, $P_{(6,33)} = 5$, $P_{(8,15)} = 1$, $P_{(8,30)} = 2$, $P_{(8,31)} = 8$, $P_{(12,27)} = 2$, $P_{(15,22)} = 1$, $P_{(16,21)} = 1$, $P_{(16,22)} = 1$, $P_{(16,23)} = 2$. The Bond partitions of G_4 for ABC_3 are given by $P_{(1,45)} = 10$, $P_{(3,41)} = 5$, $P_{(4,40)} = 5$, $P_{(5,24)} = 1$, $P_{(5,35)} = 1$, $P_{(6,37)} = 5$, $P_{(8,36)} = 1$, $P_{(9,35)} = 9$, $P_{(10,18)} = 1$, $P_{(13,32)} = 1$, $P_{(14,30)} = 1$, $P_{(14,31)} = 1$, $P_{(17,26)} = 1$, $P_{(17,27)} = 1$, $P_{(18,25)} = 1$, $P_{(19,24)} = 1$, $P_{(19,26)} = 1$. The Bond partitions of G_4 for ABC_4 are given by $P_{(3,5)} = 2$, $P_{(3,6)} = 6$, $P_{(3,7)} = 2$, $P_{(5,6)} = 4$, $P_{(6,6)} = 6$, $P_{(6,7)} = 8$, $P_{(6,8)} = 10$, $P_{(7,8)} = 3$, $P_{(7,8)} = 3$, $P_{(7,9)} = 2$, $P_{(8,8)} = 2$, $P_{(8,9)} = 1$. The Bond partitions of G_4 for ABC_5 are given by $P_{(8,8)} = 1$, $P_{(8,9)} = 3$, $P_{(9,9)} = 1$, $P_{(9,10)} = 7$, $P_{(10,10)} = 1$, $P_{(10,11)} = 8$, $P_{(11,12)} = 6$, $P_{(11,13)} = 1$, $P_{(12,13)} = 6$, $P_{(13,14)} = 4$, $P_{(14,15)} = 5$. The Bond partitions of G_4 for ABC_6 are given by $P_{(2,2)} = 2$, $P_{(2,3)} = 6$, $P_{(2,4)} = 6$, $P_{(3,4)} = 8$, $P_{(3,5)} = 4$, $P_{(4,4)} = 6$, $P_{(4,5)} = 9$, $P_{(4,6)} = 2$, $P_{(5,5)} = 2$, $P_{(5,6)} = 1$.

Chloroquine:
Chloroquine is an aminoquinoline used for the prevention and therapy of malaria. It is also effective in extraintestinal amebiasis and as an antiinflammatory agent for therapy of rheumatoid arthritis and lupus erythematosus. Chloroquine is not associated with serum enzyme elevations and is an extremely rare cause of clinically apparent acute liver injury. G_5 be the molecular graph of Chloroquine (Figure 2). The molecular graph has 22 atoms (vertices) and 23 bonds (edges). For more detail, see [49, 50, 53]. Bond partitions of G_5 for ABC_1 are given by $P_{(1,2)} = 2$, $P_{(1,3)} = 2$, $P_{(2,2)} = 5$, $P_{(2,3)} = 12$, $P_{(3,3)} = 2$. Bond partitions of G_5 for ABC_2 are given by $P_{(1,19)} = 2$, $P_{(1,20)} = 4$, $P_{(2,18)} = 2$, $P_{(3,17)} = 4$, $P_{(4,16)} = 2$, $P_{(5,15)} = 4$, $P_{(6,14)} = 1$, $P_{(7,13)} = 3$, $P_{(9,11)} = 1$, $P_{(10,10)} = 1$. The Bond partitions of G_5 for ABC_3 are given by $P_{(1,21)} = 2$, $P_{(1,22)} = 4$, $P_{(2,19)} = 1$, $P_{(3,18)} = 4$, $P_{(4,17)} = 1$, $P_{(5,15)} = 3$, $P_{(5,16)} = 1$, $P_{(6,15)} = 1$, $P_{(7,14)} = 2$, $P_{(8,13)} = 1$, $P_{(9,13)} = 1$, $P_{(10,12)} = 1$. The Bond partitions of G_5 for ABC_4 are given by $P_{(2,4)} = 2$, $P_{(3,5)} = 2$, $P_{(4,5)} = 4$, $P_{(4,6)} = 2$, $P_{(5,5)} = 3$, $P_{(5,6)} = 3$, $P_{(5,7)} = 2$, $P_{(5,8)} = 1$, $P_{(6,7)} = 2$, $P_{(7,8)} = 2$. The Bond partitions of G_5 for ABC_5 are given by $P_{(7,7)} = 1$, $P_{(7,8)} = 3$, $P_{(8,9)} = 3$, $P_{(9,10)} = 4$, $P_{(10,11)} = 5$, $P_{(11,12)} = 4$, $P_{(12,13)} = 3$. The Bond partitions of G_5 for ABC_6 are given by $P_{(1,2)} = 2$, $P_{(2,2)} = 2$, $P_{(2,3)} = 8$, $P_{(2,4)} = 1$, $P_{(3,3)} = 2$, $P_{(3,4)} = 3$, $P_{(3,5)} = 1$, $P_{(4,4)} = 2$, $P_{(4,5)} = 2$.

Hydroxychloroquine:

Hydroxychloroquine is a derivative of chloroquine that has both antimalarial and antiinflammatory activities and is now most often used as an antirheumatologic agent in systemic lupus erythematosis and rheumatoid arthritis. Hydroxychloroquine therapy has not been associated with liver function abnormalities and is an extremely rare cause of clinically apparent acute liver injury. G_6 be the molecular graph of Hydroxychloroquine (Figure 2). The molecular graph has 23 atoms (vertices) and 24 bonds (edges). For more detail, see [51, 53].
Bond partitions of G_6 for ABC_1 are given by $P_{(1,2)} = 2$, $P_{(1,3)} = 2$,$P_{(2,2)} = 6$, $P_{(2,3)} = 12$, $P_{(3,3)} = 2$. Bond partitions of G_6 for ABC_2 are given by $P_{(1,20)} = 2$, $P_{(1,21)} = 4$, $P_{(2,19)} = 3$, $P_{(3,18)} = 4$, $P_{(5,16)} = 4$, $P_{(6,15)} = 1$,$P_{(7,14)} = 3$, $P_{(10,11)} = 2$, $P_{(8,13)} = 1$. Bond partitions of G_6 for ABC_3 are given by $P_{(1,22)} = 2$, $P_{(1,23)} = 4$, $P_{(2,20)} = 2$, $P_{(2,21)} = 1$, $P_{(3,19)} = 4$, $P_{(5,16)} = 3$, $P_{(5,17)} = 1$, $P_{(6,16)} = 1$, $P_{(7,15)} = 1$, $P_{(8,14)} = 3$, $P_{(10,13)} = 1$, $P_{(11,12)} = 1$. Bond partitions of G_6 for ABC_4 are given by $P_{(2,3)} = 1$, $P_{(2,4)} = 1$, $P_{(3,5)} = 3$, $P_{(4,5)} = 4$, $P_{(4,6)} = 1$, $P_{(5,5)} = 3$, $P_{(5,6)} = 4$, $P_{(5,7)} = 2$, $P_{(5,8)} = 1$, $P_{(6,7)} = 2$, $P_{(7,8)} = 2$. Bond partitions of G_6 for ABC_5 are given by $P_{(7,8)} = 3$, $P_{(8,9)} = 2$, $P_{(9,10)} = 3$, $P_{(10,11)} = 4$, $P_{(11,12)} = 6$, $P_{(12,13)} = 4$, $P_{(13,14)} = 2$. Bond partitions of G_6 for ABC_6 are given by $P_{(1,1)} = 1$, $P_{(1,2)} = 1$, $P_{(1,3)} = 1$, $P_{(2,2)} = 2$, $P_{(2,3)} = 8$, $P_{(2,4)} = 1$, $P_{(3,3)} = 2$, $P_{(3,4)} = 3$, $P_{(3,5)} = 1$, $P_{(4,4)} = 2$, $P_{(4,5)} = 2$.

Lopinavir:
Lopinavir is a peptidomimetic HIV protease inhibitor that retains activity against HIV protease with the Val 82 mutation. Lopinavir is less affected by binding to serum proteins than the structurally-related drug ritonavir. G_7 be the molecular graph of Lopinavir (Figure 2). The molecular graph has 46 atoms (vertices) and 49 bonds (edges). For more detail, see [31, 53]. The Bond partitions of G_7 for ABC_1 are given by $P_{(1,3)} = 8$, $P_{(2,2)} = 14$, $P_{(2,3)} = 20$,$P_{(3,3)} = 7$. Bond partitions of G_7 for ABC_2 are given by $P_{(1,44)} = 8$, $P_{(2,42)} = 20$, $P_{(3,41)} = 5$, $P_{(5,39)} = 2$, $P_{(6,38)} = 3$, $P_{(7,37)} = 1$, $P_{(8,36)} = 1$, $P_{(9,35)} = 1$, $P_{(10,34)} = 2$, $P_{(11,33)} = 1$, $P_{(12,32)} = 1$, $P_{(13,31)} = 1$, $P_{(20,24)} = 1$, $P_{(21,23)} = 1$, $P_{(22,22)} = 1$. Bond partitions of G_7 for ABC_3 are given by $P_{(1,48)} = 8$, $P_{(2,45)} = 21$, $P_{(3,44)} = 4$, $P_{(6,42)} = 2$, $P_{(7,41)} = 3$, $P_{(8,40)} = 1$, $P_{(9,39)} = 1$, $P_{(10,38)} = 1$, $P_{(11,37)} = 1$, $P_{(12,36)} = 1$, $P_{(13,35)} = 2$, $P_{(14,34)} = 1$, $P_{(22,26)} = 1$, $P_{(24,24)} = 1$, $P_{(25,23)} = 1$. Bond partitions of G_7 for ABC_4 are given by $P_{(3,5)} = 3$, $P_{(3,6)} = 6$, $P_{(4,4)} = 5$, $P_{(4,5)} = 8$, $P_{(5,5)} = 2$, $P_{(5,6)} = 7$, $P_{(5,8)} = 2$, $P_{(5,9)} = 1$, $P_{(6,6)} = 7$, $P_{(6,7)} = 3$, $P_{(6,8)} = 3$, $P_{(6,9)} = 1$, $P_{(8,9)} = 1$. Bond partitions of G_7 for ABC_5 are given by $P_{(9,10)} = 3$, $P_{(10,11)} = 3$, $P_{(11,12)} = 4$, $P_{(12,13)} = 6$, $P_{(13,14)} = 7$, $P_{(14,15)} = 7$ $P_{(15,16)} = 8$, $P_{(16,17)} = 7$, $P_{(17,18)} = 4$. Bond partitions of G_7 for ABC_6 are given by $P_{(2,2)} = 8$, $P_{(2,3)} = 14$, $P_{(2,4)} = 1$, $P_{(2,6)} = 1$, $P_{(3,3)} = 8$, $P_{(3,4)} = 8$, $P_{(3,5)} = 5$, $P_{(3,6)} = 1$, $P_{(4,4)} = 2$, $P_{(5,6)} = 1$.

Arbidol:
Arbidol is an orally bioavailable indole derivative, with broad-spectrum antiviral and potential anti-inflammatory activities. Upon oral administration, Arbidol inhibits the fusion of the viral envelope with host cell membrane, thereby blocking the entry of virus into host cells and preventing viral infection and replica-

tion. Arbidol may also suppress the expression of the cytokines interleukin-1beta (IL-1b), IL-6, IL-12 and tumor necrosis factor-alpha (TNF-a) and promote the expression of IL-10. This may reduce inflammation. G_8 be the molecular graph of Arbidol (Figure 3). The molecular graph has 29 atoms (vertices) and 31 bonds (edges). For more detail, see [36, 53].

Bond partitions of G_8 for ABC_1 are given by $P_{(1,2)} = 1$, $P_{(1,3)} = 6$,$P_{(2,2)} = 6$, $P_{(2,3)} = 9$, $P_{(3,3)} = 9$. Bond partitions of G_8 for ABC_2 are given by $P_{(1,26)} = 1$, $P_{(1,27)} = 7$, $P_{(2,25)} = 8$, $P_{(3,24)} = 1$, $P_{(4,23)} = 3$, $P_{(5,13)} = 2$,$P_{(5,22)} = 1$, $P_{(6,21)} = 1$, $P_{(7,20)} = 1$, $P_{(8,19)} = 2$, $P_{(10,11)} = 1$, $P_{(10,16)} = 1$, $P_{(11,14)} = 2$. Bond partitions of G_8 for ABC_3 are given by $P_{(1,29)} = 1$, $P_{(1,30)} = 7$, $P_{(2,27)} = 6$, $P_{(2,28)} = 2$, $P_{(3,27)} = 1$, $P_{(4,25)} = 2$, $P_{(4,26)} = 1$. $P_{(5,24)} = 1$, $P_{(6,14)} = 2$, $P_{(6,24)} = 1$, $P_{(7,16)} = 1$, $P_{(7,23)} = 1$, $P_{(8,21)} = 2$, $P_{(8,22)} = 1$, $P_{(12,13)} = 1$, $P_{(12,14)} = 1$. Bond partitions of G_8 for ABC_4 are given by $P_{(2,3)} = 1$, $P_{(3,4)} = 2$, $P_{(3,5)} = 1$, $P_{(3,6)} = 2$, $P_{(3,7)} = 2$, $P_{(4,4)} = 2$, $P_{(4,5)} = 2$, $P_{(4,6)} = 1$, $P_{(5,5)} = 1$, $P_{(5,6)} = 4$, $P_{(5,8)} = 1$, $P_{(6,6)} = 1$, $P_{(6,7)} = 1$, $P_{(6,8)} = 2$, $P_{(6,9)} = 1$, $P_{(7,8)} = 3$, $P_{(8,9)} = 3$, $P_{(9,9)} = 1$. Bond partitions of G_8 for ABC_5 are given by $P_{(6,7)} = 3$, $P_{(7,8)} = 5$, $P_{(8,8)} = 1$, $P_{(8,9)} = 5$, $P_{(9,10)} = 6$, $P_{(10,10)} = 1$, $P_{(10,11)} = 6$, $P_{(11,12)} = 4$. Bond partitions of G_8 for ABC_6 are given by $P_{(1,1)} = 1$, $P_{(1,2)} = 2$, $P_{(1,3)} = 1$, $P_{(1,4)} = 1$, $P_{(2,2)} = 2$, $P_{(2,3)} = 4$, $P_{(2,4)} = 2$, $P_{(3,3)} = 5$, $P_{(3,4)} = 2$, $P_{(3,5)} = 1$, $P_{(3,6)} = 1$, $P_{(4,5)} = 5$, $P_{(5,6)} = 3$, $P_{(6,6)} = 1$.

Ritonavir:
Ritonavir is a peptidomimetic agent that inhibits both HIV-1 and HIV-2 proteases. Ritonavir is highly inhibited by serum proteins but boosts the effect of other HIV proteases by blocking their degradation by cytochrome P450. G_9 be the molecular graph of Ritonavir (Figure 3). The molecular graph has 50 atoms (vertices) and 53 bonds (edges). For more detail, see [31, 53].
Bond partitions of G_9 for ABC_1 are given by $P_{(1,3)} = 9$, $P_{(2,2)} = 16$, $P_{(2,3)} = 23$, $P_{(3,3)} = 5$. Bond partitions of G_9 for ABC_2 are given by $P_{(1,1)} = 1$, $P_{(1,4)} = 1$, $P_{(1,43)} = 5$, $P_{(1,46)} = 9$, $P_{(1,48)} = 14$, $P_{(2,46)} = 1$, $P_{(4,44)} = 2$, $P_{(5,43)} = 3$, $P_{(6,42)} = 3$, $P_{(7,41)} = 1$, $P_{(8,40)} = 2$, $P_{(9,39)} = 1$, $P_{(10,38)} = 1$, $P_{(12,36)} = 1$, $P_{(13,35)} = 1$, $P_{(17,31)} = 2$, $P_{(19,29)} = 2$, $P_{(20,28)} = 2$. Bond partitions of G_9 for ABC_3 are given by $P_{(1,52)} = 9$, $P_{(2,2)} = 1$, $P_{(2,5)} = 1$, $P_{(2,47)} = 1$, $P_{(2,50)} = 18$, $P_{(5,46)} = 1$, $P_{(5,47)} = 3$, $P_{(6,46)} = 3$, $P_{(7,45)} = 3$, $P_{(8,44)} = 1$, $P_{(9,41)} = 1$, $P_{(9,43)} = 1$, $P_{(10,42)} = 1$, $P_{(11,41)} = 1$, $P_{(13,39)} = 1$, $P_{(14,38)} = 1$, $P_{(18,34)} = 1$, $P_{(20,32)} = 2$, $P_{(21,31)} = 2$, $P_{(22,30)} = 1$. Bond partitions of G_9 for ABC_4 are given by $P_{(3,5)} = 5$, $P_{(3,6)} = 4$, $P_{(4,4)} = 5$, $P_{(4,5)} = 6$, $P_{(5,5)} = 3$, $P_{(5,6)} = 10$, $P_{(5,7)} = 3$, $P_{(5,8)} = 1$, $P_{(6,6)} = 11$, $P_{(6,7)} = 3$, $P_{(6,8)} = 2$. Bond partitions of G_9 for ABC_5 are given by $P_{(11,12)} = 2$, $P_{(12,13)} = 4$, $P_{(13,14)} = 4$, $P_{(14,15)} = 7$, $P_{(15,16)} = 6$, $P_{(16,17)} = 6$,$P_{(17,18)} = 5$, $P_{(18,19)} = 5$, $P_{(19,20)} = 5$, $P_{(20,20)} = 1$, $P_{(20,21)} = 3$, $P_{(21,22)} = 4P_{(22,22)} = 1$. Bond partitions of G_9 for ABC_6 are given by $P_{(2,2)} = 10$, $P_{(2,3)} = 11$, $P_{(2,4)} = 2$, $P_{(2,5)} = 1$, $P_{(3,3)} = 12$, $P_{(3,4)} = 13$, $P_{(3,5)} = 1$, $P_{(4,4)} = 2$, $P_{(4,5)} = 1$.

Thalidomide:
Thalidomide and its analogue lenalidomide are immunomodulatory and antineo-

plastic agents that are used in the therapy of multiple myeloma. Both agents are associated with a low rate of serum aminotransferase elevations during therapy and both have been implicated in causing rare instances of clinically apparent liver injury which can be severe. G_{10} be the molecular graph of Thalidomide (Figure 1). The molecular graph has 19 atoms (vertices) and 21 bonds (edges). For more detail, see [37, 53]. Bond partitions of G_{10} for ABC_1 are given by $P_{(1,3)} = 4$, $P_{(2,2)} = 4$, $P_{(2,3)} = 6$, $P_{(3,3)} = 7$. Bond partitions of G_{10} for ABC_2 are given by $P_{(1,17)} = 4$, $P_{(2,15)} = 4$, $P_{(3,14)} = 5$, $P_{(4,4)} = 2$, $P_{(4,13)} = 1$, $P_{(5,10)} = 2$, $P_{(6,10)} = 2$, $P_{(7,10)} = 1$. Bond partitions of G_4 for ABC_{10} are given by $P_{(1,20)} = 4$, $P_{(2,17)} = 4$, $P_{(3,16)} = 4$, $P_{(4,15)} = 2$, $P_{(5,5)} = 2$, $P_{(5,13)} = 1$, $P_{(6,12)} = 1$, $P_{(8,12)} = 1$, $P_{(7,12)} = 2$. Bond partitions of G_{10} for ABC_4 are given by $P_{(3,5)} = 1$, $P_{(3,6)} = 1$, $P_{(3,7)} = 2$, $P_{(4,4)} = 1$, $P_{(4,5)} = 2$, $P_{(5,5)} = 2$, $P_{(5,6)} = 1$, $P_{(5,8)} = 3$, $P_{(6,6)} = 1$, $P_{(6,8)} = 1$, $P_{(7,8)} = 2$, $P_{(7,9)} = 2$, $P_{(8,8)} = 1$, $P_{(8,9)} = 1$. Bond partitions of G_{10} for ABC_5 are given by $P_{(5,5)} = 1$, $P_{(5,6)} = 4$, $P_{(6,7)} = 7$, $P_{(7,7)} = 1$, $P_{(7,8)} = 4$, $P_{(8,9)} = 3$, $P_{(9,9)} = 1$. Bond partitions of G_{10} for ABC_6 are given by $P_{(2,2)} = 2$, $P_{(2,3)} = 4$, $P_{(2,4)} = 3$, $P_{(3,3)} = 1$, $P_{(3,4)} = 1$, $P_{(3,5)} = 4$, $P_{(4,5)} = 2$, $P_{(4,6)} = 2$, $P_{(5,5)} = 1$, $P_{(5,6)} = 1$.

Histidine:
L-histidine is the L-enantiomer of the amino acid histidine. It has a role as a nutraceutical, a micronutrient, a Saccharomyces cerevisiae metabolite, an Escherichia coli metabolite, a human metabolite, an algal metabolite and a mouse metabolite. It is a proteinogenic amino acid, a histidine and a L-alpha-amino acid. It is a conjugate base of a L-histidinium(1+). It is a conjugate acid of a L-histidinate(1-). It is an enantiomer of a D-histidine. It is a tautomer of a L-histidine zwitterion. G_{11} be the molecular graph of Histidine (Figure 3). The molecular graph has 15 atoms (vertices) and 15 bonds (edges). For more detail, see [38,53]. Bond partitions of G_{11} for ABC_1 are given by $P_{(1,2)} = 1$, $P_{(1,3)} = 4$, $P_{(2,2)} = 2$, $P_{(2,3)} = 5$, $P_{(3,3)} = 3$. Bond partitions of G_{11} for ABC_2 are given by $P_{(1,2)} = 1$, $P_{(1,10)} = 1$, $P_{(1,11)} = 2$, $P_{(1,12)} = 1$, $P_{(1,13)} = 5$, $P_{(2,9)} = 1$, $P_{(2,11)} = 1$, $P_{(3,10)} = 1$, $P_{(6,7)} = 1$, $P_{(5,8)} = 1$. Bond partitions of G_{11} for ABC_3 are given by $P_{(1,13)} = 1$, $P_{(1,14)} = 5$, $P_{(2,3)} = 1$, $P_{(2,11)} = 2$, $P_{(2,12)} = 1$, $P_{(3,11)} = 2$, $P_{(6,8)} = 1$, $P_{(7,7)} = 1$, $P_{(5,9)} = 1$. Bond partitions of G_{11} for ABC_4 are given by $P_{(2,4)} = 1$, $P_{(3,5)} = 2$, $P_{(3,6)} = 2$, $P_{(4,5)} = 2$, $P_{(4,6)} = 1$, $P_{(5,6)} = 1$, $P_{(5,7)} = 1$, $P_{(5,8)} = 1$, $P_{(6,7)} = 2$, $P_{(6,8)} = 2$. Bond partitions of G_{11} for ABC_5 are given by $P_{(4,4)} = 1$, $P_{(4,5)} = 3$, $P_{(5,6)} = 6$, $P_{(6,7)} = 4$, $P_{(7,7)} = 1$. Bond partitions of G_{11} for ABC_6 are given by $P_{(1,2)} = 1$, $P_{(2,2)} = 2$, $P_{(2,3)} = 5$, $P_{(2,4)} = 1$, $P_{(3,3)} = 1$, $P_{(3,4)} = 3$, $P_{(4,4)} = 2$.

2-Phenoxyethanol:
Phenoxyethanol is a colorless liquid with a pleasant odor. It is a glycol ether used as a perfume fixative, insect repellent, antiseptic, solvent, preservative, and also as an anesthetic in fish aquaculture. Phenoxyethanol is an ether alcohol with aromatic properties. It is both naturally found and manufactured synthetically. Demonstrating antimicrobial ability, phenoxyethanol acts as an effective preservative in pharmaceuticals, cosmetics and lubricants. G_{12} be the

molecular graph of 2-Phenoxyethanol (Figure 3). The molecular graph has 11 atoms (vertices) and 11 bonds (edges). For more detail, see [39, 53].

Bond partitions of G_{12} for ABC_1 are given by $P_{(1,2)} = 1$, $P_{(2,2)} = 7$, $P_{(2,3)} = 3$. Bond partitions of G_{12} for ABC_2 are given by $P_{(1,8)} = 1$, $P_{(1,9)} = 1$, $P_{(2,7)} = 7$, $P_{(3,6)} = 1$, $P_{(4,5)} = 1$. Bond partitions of G_{12} for ABC_3 are given by $P_{(1,9)} = 1$, $P_{(1,10)} = 1$, $P_{(2,7)} = 6$, $P_{(2,8)} = 1$, $P_{(3,7)} = 1$, $P_{(4,6)} = 1$. Bond partitions of G_{12} for ABC_4 are given by $P_{(2,3)} = 1$, $P_{(3,4)} = 1$, $P_{(4,4)} = 3$, $P_{(4,5)} = 3$, $P_{(5,6)} = 3$. Bond partitions of G_{12} for ABC_5 are given by $P_{(4,5)} = 2$, $P_{(5,6)} = 3$, $P_{(6,7)} = 3$, $P_{(7,8)} = 3$. Bond partitions of G_6 for ABC_6 are given by $P_{(1,1)} = 1$, $P_{(1,2)} = 1$, $P_{(2,2)} = 3$, $P_{(2,3)} = 3$, $P_{(3,3)} = 3$.
From the above bond partition, the computation of ABC_i can be done for the molecular graphs.

4 Computational methods

This section provides the computational results of ABC indices and polynomials of the molecular structures. From the bond partitions of Favipiravir the ABC indices and polynomials are obtained as shown below:

$$\begin{aligned}
ABC_1(G_1) &= \sum_{j=1}^{k} \sqrt{\frac{d(u)+d(v)-2}{d(u)d(v)}} \\
&= 8\sqrt{\frac{1+3-2}{3}} + 14\sqrt{\frac{2+2-2}{4}} + 20\sqrt{\frac{2+3-2}{6}} + 7\sqrt{\frac{3+3-2}{9}} \\
&= 8.13485
\end{aligned}$$

$$ABC_2(G_1) = \sum_{uv\in E(G)} \sqrt{\frac{n(u)+n(v)-2}{n(u).n(v)}} = 8.22$$

$$ABC_3(G_1) = \sum_{uv\in E(G)} \sqrt{\frac{m(u)+m(v)-2}{m(u).m(v)}} = 8.2435$$

$$ABC_4(G_1) = \sum_{uv\in E(G)} \sqrt{\frac{s(u)+s(v)-2}{s(u).s(v)}} = 6.2722$$

$$ABC_5(G_1) = \sum_{uv\in E(G)} \sqrt{\frac{e(u)+e(v)-2}{e(u).e(v)}} = 6.76518$$

$$ABC_6(G_1) = \sum_{uv\in E(G)} \sqrt{\frac{d_2(u)+d_2(v)-2}{d_2(u).d_2(v)}} = 7.50714$$

The ABC polynomials of a graph G_1 is

$$\begin{aligned}
ABC_i(G,x) &= \sum_{j=1}^{k} x^{\sqrt{\frac{x_i+y_i-2}{x_i y_i}}} \\
ABC_1(G_1,x) &= 4x^{\sqrt{\frac{2}{3}}} + x^{\sqrt{\frac{2}{4}}} + 4x^{\sqrt{\frac{3}{6}}} + 2x^{\sqrt{\frac{4}{9}}} \\
&= 4x^{\sqrt{\frac{2}{3}}} + 5x^{\frac{1}{\sqrt{2}}} + 2x^{\frac{2}{3}} \\
ABC_2(G_1,x) &= 4x^{\frac{2\sqrt{2}}{3}} + x^{\frac{1}{\sqrt{2}}} + 6x^{\frac{\sqrt{7}}{3\sqrt{2}}} \\
ABC_3(G_1,x) &= 4x^{\frac{3}{\sqrt{10}}} + x^{\frac{1}{\sqrt{2}}} + 6x^{\frac{\sqrt{7}}{3\sqrt{2}}} \\
ABC_4(G_1,x) &= 3x^{\sqrt{\frac{2}{5}}} + x^{\frac{\sqrt{7}}{3\sqrt{2}}} + 2x^{\frac{2\sqrt{2}}{5}} + 2x^{\frac{3}{\sqrt{30}}} + x^{\frac{\sqrt{11}}{2\sqrt{10}}} + 2x^{\frac{1}{2}} \\
ABC_5(G_1,x) &= x^{\frac{2}{3}} + 3x^{\frac{\sqrt{5}}{2\sqrt{3}}} + x^{\frac{\sqrt{6}}{4}} + 6x^{\frac{\sqrt{7}}{2\sqrt{5}}} \\
ABC_6(G_1,x) &= 7x^{\frac{1}{\sqrt{2}}} + 2x^{\frac{2}{3}} + x^{\sqrt{\frac{2}{5}}} + x^{\frac{\sqrt{7}}{2\sqrt{5}}}
\end{aligned}$$

Similarly, we obtain the ABC indices and polynomials for the remaining molecular graphs. for convenience, the computed values of ABC indices and Polynomial expressions of remaining graphs are represented in the Table format.

Molecular graphs	ABC_2 Descriptor	ABC_2 polynomials
G_1	8.22	$4x^{\frac{2\sqrt{2}}{3}} + x^{\frac{1}{\sqrt{2}}} + 6x^{\frac{\sqrt{7}}{3\sqrt{2}}}$
G_2	13.4584	$x^{\sqrt{\frac{3}{2}}} + x^{\frac{3}{\sqrt{10}}} + x^{\sqrt{\frac{13}{14}}} + 5x^{\sqrt{\frac{14}{15}}} + 2x^{\frac{1}{\sqrt{2}}} + x^{\frac{\sqrt{10}}{3\sqrt{3}}}$ $+x^{\sqrt{\frac{11}{30}}} + x^{\frac{\sqrt{11}}{6}} + 3x^{\sqrt{\frac{3}{10}}} + x^{\frac{\sqrt{13}}{2\sqrt{11}}} + x^{\sqrt{\frac{13}{56}}}$
G_3	28.0076	$x^{\sqrt{\frac{5}{6}}} + x^{\sqrt{\frac{33}{34}}} + 2x^{\sqrt{\frac{37}{38}}} + 9x^{\sqrt{\frac{38}{39}}} + 8x^{\sqrt{\frac{37}{74}}} + x^{\frac{\sqrt{13}}{6}} + x^{\frac{2\sqrt{6}}{\sqrt{69}}} + 2x^{\frac{\sqrt{37}}{6\sqrt{3}}} + x^{\frac{\sqrt{34}}{8\sqrt{2}}} + x^{\frac{\sqrt{35}}{2\sqrt{33}}} + x^{\frac{3}{\sqrt{34}}} + x^{\frac{\sqrt{37}}{2\sqrt{35}}} + x^{\sqrt{\frac{37}{170}}} + x^{\frac{3}{4\sqrt{3}}} + 2x^{\frac{\sqrt{37}}{3\sqrt{22}}}$ $+x^{\frac{\sqrt{37}}{2\sqrt{62}}} + x^{\frac{\sqrt{37}}{3\sqrt{30}}} + x^{\sqrt{\frac{37}{290}}} + x^{\frac{\sqrt{37}}{2\sqrt{77}}} + x^{\frac{\sqrt{17}}{12}} + x^{\frac{\sqrt{35}}{2\sqrt{78}}} + x^{\frac{6}{5\sqrt{13}}} + x^{\sqrt{\frac{37}{374}}} + x^{\frac{\sqrt{37}}{3\sqrt{42}}} + x^{\frac{\sqrt{37}}{2\sqrt{95}}}$
G_4	25.6476	$10x^{\frac{\sqrt{39}}{2\sqrt{10}}} + 5x^{\frac{\sqrt{37}}{6\sqrt{3}}} + x^{\frac{\sqrt{23}}{2\sqrt{21}}} + x^{\frac{2}{\sqrt{15}}} + 6x^{\frac{\sqrt{37}}{2\sqrt{35}}} + 5x^{\frac{\sqrt{37}}{3\sqrt{22}}} + x^{\frac{\sqrt{21}}{2\sqrt{30}}}$ $+2x^{\frac{3}{2\sqrt{15}}} + 8x^{\frac{\sqrt{37}}{2\sqrt{62}}} + 2x^{\frac{\sqrt{37}}{18}} + x^{\sqrt{\frac{35}{330}}} + x^{\frac{\sqrt{35}}{4\sqrt{21}}} + x^{\frac{3}{2\sqrt{22}}} + 2x^{\frac{\sqrt{37}}{4\sqrt{23}}}$
G_5	14.7737	$2x^{\frac{3\sqrt{2}}{\sqrt{19}}} + 4x^{\frac{\sqrt{19}}{2\sqrt{5}}} + 2x^{\frac{1}{\sqrt{2}}} + 4x^{\frac{3\sqrt{2}}{\sqrt{51}}} + x^{\frac{3\sqrt{2}}{8}} + 4x^{\frac{\sqrt{6}}{5}} + x^{\frac{3}{\sqrt{42}}} + 3x^{\frac{3\sqrt{2}}{\sqrt{91}}} + x^{\sqrt{\frac{2}{11}}} + x^{\frac{3\sqrt{2}}{10}}$
G_6	15.3984	$2x^{\frac{\sqrt{19}}{2\sqrt{5}}} + 4x^{\frac{2\sqrt{5}}{\sqrt{21}}} + 3x^{\frac{1}{\sqrt{2}}} + 4x^{\frac{\sqrt{19}}{3\sqrt{6}}} + 4x^{\frac{\sqrt{19}}{4\sqrt{5}}} + 3x^{\frac{\sqrt{19}}{3\sqrt{10}}} + 2x^{\frac{\sqrt{19}}{7\sqrt{2}}} + x^{\sqrt{\frac{19}{110}}} + x^{\frac{\sqrt{19}}{2\sqrt{26}}}$
G_7	30.9199	$8x^{\frac{\sqrt{43}}{2\sqrt{11}}} + 20x^{\frac{\sqrt{42}}{2\sqrt{21}}} + 5x^{\sqrt{\frac{43}{123}}} + 2x^{\sqrt{\frac{42}{195}}} + 3x^{\frac{\sqrt{42}}{2\sqrt{57}}} + x^{\sqrt{\frac{42}{259}}} + x^{\frac{\sqrt{42}}{12\sqrt{2}}} + x^{\frac{\sqrt{42}}{3\sqrt{35}}} + 2x^{\frac{\sqrt{42}}{2\sqrt{85}}}$ $+x^{\frac{\sqrt{42}}{11\sqrt{3}}} + x^{\frac{\sqrt{42}}{8\sqrt{6}}} + x^{\sqrt{\frac{42}{403}}} + x^{\frac{\sqrt{42}}{4\sqrt{30}}} + x^{\sqrt{\frac{42}{483}}} + x^{\frac{\sqrt{42}}{22}}$
G_8	20.3836	$x^{\frac{5}{\sqrt{26}}} + 7x^{\frac{\sqrt{26}}{3\sqrt{3}}} + 8x^{\frac{1}{\sqrt{2}}} + x^{\frac{5}{6\sqrt{2}}} + 3x^{\frac{5}{2\sqrt{23}}} + 2x^{\frac{4}{\sqrt{65}}} + x^{\frac{5}{\sqrt{110}}} + x^{\frac{5}{3\sqrt{14}}}$ $+x^{\frac{5}{2\sqrt{35}}} + 2x^{\frac{5}{2\sqrt{38}}} + x^{\sqrt{\frac{19}{110}}} + x^{\frac{\sqrt{15}}{10}} + 2x^{\sqrt{\frac{23}{154}}}$
G_9	38.7279	$1 + x^{\sqrt{\frac{3}{4}}} + 5x^{\sqrt{\frac{42}{43}}} + 9x^{\frac{3\sqrt{5}}{\sqrt{46}}} + 14x^{\frac{\sqrt{42}}{4\sqrt{3}}} + x^{\frac{\sqrt{46}}{2\sqrt{23}}} + x^{\frac{3\sqrt{5}}{2\sqrt{43}}}$ $+2x^{\frac{\sqrt{46}}{4\sqrt{11}}} + 3x^{\sqrt{\frac{46}{215}}} + 3x^{\frac{\sqrt{46}}{6\sqrt{7}}} + x^{\sqrt{\frac{46}{287}}} + 2x^{\frac{\sqrt{46}}{8\sqrt{5}}} + x^{\frac{\sqrt{46}}{3\sqrt{39}}} + x^{\frac{\sqrt{46}}{2\sqrt{95}}} + x^{\frac{\sqrt{46}}{12\sqrt{3}}} + x^{\sqrt{\frac{46}{455}}} + 2x^{\sqrt{\frac{46}{527}}} + 2x^{\sqrt{\frac{46}{551}}} + 2x^{\frac{\sqrt{46}}{4\sqrt{35}}}$
G_{10}	13.9077	$4x^{\frac{4}{\sqrt{17}}} + 4x^{\frac{1}{\sqrt{2}}} + 5x^{\sqrt{\frac{15}{42}}} + 2x^{\frac{\sqrt{6}}{4}} + x^{\frac{\sqrt{15}}{2\sqrt{13}}} + 2x^{\frac{\sqrt{13}}{5\sqrt{2}}} + 2x^{\frac{\sqrt{14}}{2\sqrt{15}}} + x^{\sqrt{\frac{15}{70}}}$
G_{11}	12.3799	$2x^{\frac{1}{\sqrt{2}}} + x^{\frac{3}{\sqrt{10}}} + 2x^{\sqrt{\frac{10}{11}}} + x^{\frac{\sqrt{11}}{2\sqrt{3}}} + 5x^{\frac{2\sqrt{3}}{\sqrt{13}}} + x^{\frac{3}{3\sqrt{2}}} + x^{\sqrt{\frac{11}{30}}} + x^{\sqrt{\frac{11}{42}}} + x^{\frac{\sqrt{11}}{2\sqrt{10}}}$
G_{12}	8.04319	$x^{\frac{\sqrt{7}}{2\sqrt{2}}} + x^{\frac{2\sqrt{2}}{3}} + 7x^{\frac{1}{\sqrt{2}}} + x^{\frac{\sqrt{7}}{3\sqrt{2}}} + x^{\frac{\sqrt{7}}{2\sqrt{5}}}$

Table 1: Polynomials of ABC_2

Molecular graphs	ABC_3 Descriptor	ABC_3 polynomials
G_1	8.2435	$4x^{\frac{3}{\sqrt{10}}} + x^{\frac{1}{\sqrt{2}}} + 6x^{\frac{\sqrt{7}}{3\sqrt{2}}}$
G_2	12.5972	$x^{\sqrt{\frac{15}{4}}} + 5x^{\frac{4}{\sqrt{17}}} + 3x^{\frac{1}{\sqrt{2}}} + x^{\frac{\sqrt{6}}{4}} + x^{\frac{\sqrt{13}}{2\sqrt{11}}} + x^{\frac{\sqrt{7}}{2\sqrt{6}}} + x^{\sqrt{\frac{14}{55}}} + 4x^{\frac{1}{2}} + x^{\frac{\sqrt{5}}{2\sqrt{6}}}$
G_3	27.5147	$2x^{\sqrt{\frac{41}{42}}} + 9x^{\sqrt{\frac{42}{43}}} + 10x^{\frac{1}{\sqrt{2}}} + 2x^{\frac{2\sqrt{10}}{3\sqrt{13}}} + x^{\frac{\sqrt{17}}{2\sqrt{15}}} + x^{\frac{\sqrt{41}}{2\sqrt{39}}} + x^{\sqrt{\frac{7}{26}}}$ $+2x^{\frac{2\sqrt{10}}{\sqrt{185}}} + x^{\sqrt{\frac{41}{190}}} + x^{\sqrt{\frac{39}{210}}} + 2x^{\sqrt{\frac{41}{222}}} + x^{\frac{\sqrt{41}}{6\sqrt{7}}} + 2x^{\frac{\sqrt{41}}{2\sqrt{70}}} + x^{\sqrt{\frac{41}{330}}}$ $+2x^{\frac{\sqrt{41}}{4\sqrt{22}}} + x^{\frac{2\sqrt{2}}{9}} + x^{\frac{\sqrt{10}}{2\sqrt{26}}} + x^{\frac{\sqrt{41}}{12\sqrt{3}}} + x^{\frac{\sqrt{41}}{2\sqrt{115}}} + 2x^{\sqrt{\frac{41}{462}}}$
G_4	24.9654	$10x^{\frac{2\sqrt{11}}{3\sqrt{5}}} + 5x^{\sqrt{\frac{42}{123}}} + 5x^{\frac{\sqrt{21}}{4\sqrt{5}}} + x^{\frac{3}{2\sqrt{10}}} + x^{\frac{\sqrt{38}}{5\sqrt{7}}} + 5x^{\sqrt{\frac{41}{222}}} + x^{\frac{\sqrt{31}}{12}}$ $+9x^{\frac{\sqrt{43}}{3\sqrt{35}}} + x^{\frac{\sqrt{26}}{6\sqrt{5}}} + x^{\frac{\sqrt{43}}{4\sqrt{26}}} + x^{\frac{\sqrt{43}}{2\sqrt{105}}} + x^{\sqrt{\frac{43}{434}}} + x^{\sqrt{\frac{41}{442}}}$ $+x^{\frac{\sqrt{42}}{3\sqrt{51}}} + x^{\frac{\sqrt{41}}{15\sqrt{2}}} + x^{\frac{\sqrt{41}}{2\sqrt{114}}} + x^{\sqrt{\frac{43}{494}}}$
G_5	14.7216	$2x^{\frac{2\sqrt{5}}{\sqrt{21}}} + 4x^{\sqrt{\frac{21}{22}}} + 2x^{\frac{1}{\sqrt{2}}} + 4x^{\frac{\sqrt{10}}{3\sqrt{6}}} + x^{\frac{\sqrt{10}}{2\sqrt{17}}} + 3x^{\frac{\sqrt{6}}{5}}$ $+x^{\frac{\sqrt{19}}{4\sqrt{5}}} + x^{\frac{\sqrt{19}}{3\sqrt{10}}} + 2x^{\frac{\sqrt{19}}{7\sqrt{2}}} + x^{\frac{\sqrt{19}}{2\sqrt{26}}} + x^{\frac{2\sqrt{5}}{3\sqrt{13}}} + x^{\frac{1}{\sqrt{6}}}$
G_6	15.2653	$2x^{\sqrt{\frac{21}{22}}} + 4x^{\sqrt{\frac{22}{23}}} + 3x^{\frac{1}{\sqrt{2}}} + 4x^{\frac{2\sqrt{5}}{\sqrt{57}}} + 3x^{\frac{\sqrt{10}}{4\sqrt{5}}} + x^{\frac{2}{\sqrt{17}}}$ $+x^{\frac{\sqrt{7}}{2\sqrt{6}}} + x^{\frac{2}{\sqrt{21}}} + 3x^{\frac{\sqrt{3}}{2\sqrt{7}}} + x^{\sqrt{\frac{21}{130}}} + x^{\frac{\sqrt{21}}{2\sqrt{33}}}$
G_7	30.5213	$8x^{\frac{\sqrt{47}}{4\sqrt{3}}} + 21x^{\frac{1}{\sqrt{2}}} + 4x^{\frac{3\sqrt{5}}{2\sqrt{33}}} + 2x^{\frac{\sqrt{46}}{6\sqrt{7}}} + 3x^{\sqrt{\frac{46}{287}}} + x^{\frac{\sqrt{46}}{8\sqrt{5}}} + x^{\frac{\sqrt{46}}{3\sqrt{39}}} + x^{\frac{\sqrt{46}}{2\sqrt{95}}}$ $+x^{\sqrt{\frac{46}{407}}} + x^{\frac{\sqrt{46}}{12\sqrt{3}}} + 2x^{\sqrt{\frac{46}{455}}} + x^{\frac{\sqrt{46}}{2\sqrt{119}}} + x^{\frac{\sqrt{46}}{2\sqrt{143}}} + x^{\frac{\sqrt{46}}{24}} + x^{\frac{\sqrt{2}}{5}}$
G_8	20.3216	$x^{\frac{2\sqrt{7}}{\sqrt{29}}} + 7x^{\sqrt{\frac{20}{30}}} + 8x^{\frac{1}{\sqrt{2}}} + x^{\frac{2\sqrt{7}}{9}} + 2x^{\frac{3\sqrt{3}}{10}} + x^{\sqrt{\frac{7}{26}}} + x^{\frac{3}{2\sqrt{10}}} + 2x^{\frac{3}{\sqrt{42}}} + x^{\frac{\sqrt{7}}{6}}$ $+x^{\frac{\sqrt{21}}{4\sqrt{7}}} + x^{\frac{2}{\sqrt{23}}} + 2x^{\frac{3}{2\sqrt{14}}} + x^{\frac{\sqrt{7}}{2\sqrt{11}}} + x^{\frac{\sqrt{23}}{2\sqrt{39}}} + x^{\frac{1}{\sqrt{7}}}$
G_9	32.1497	$9x^{\frac{\sqrt{11}}{2\sqrt{13}}} + 21x^{\frac{1}{\sqrt{2}}} + x^{\frac{7}{\sqrt{230}}} + 3x^{\frac{5\sqrt{2}}{\sqrt{235}}} + 3x^{\frac{5}{\sqrt{138}}} + 3x^{\frac{5\sqrt{2}}{3\sqrt{35}}} + x^{\frac{5}{4\sqrt{11}}} + x^{\frac{4\sqrt{3}}{3\sqrt{41}}}$ $+x^{\frac{5\sqrt{2}}{3\sqrt{43}}} + x^{\frac{5\sqrt{2}}{2\sqrt{105}}} + x^{\frac{5\sqrt{2}}{\sqrt{451}}} + x^{\frac{5\sqrt{2}}{13\sqrt{3}}} + x^{\frac{5\sqrt{2}}{2\sqrt{133}}} + x^{\frac{5\sqrt{2}}{6\sqrt{17}}} + 2x^{\frac{5}{8\sqrt{5}}} + 2x^{\frac{5\sqrt{2}}{2\sqrt{651}}} + x^{\frac{5\sqrt{2}}{2\sqrt{165}}}$
G_{10}	13.587	$4x^{\frac{\sqrt{19}}{2\sqrt{5}}} + 4x^{\frac{1}{\sqrt{2}}} + 4x^{\frac{\sqrt{17}}{4\sqrt{3}}} + 2x^{\frac{\sqrt{17}}{2\sqrt{15}}} + 2x^{\frac{2\sqrt{2}}{5}} + x^{\frac{4}{\sqrt{65}}} + x^{\frac{4}{6\sqrt{2}}} + x^{\frac{\sqrt{17}}{2\sqrt{21}}} + 2x^{\frac{\sqrt{3}}{4}}$
G_{11}	11.3246	$x^{\frac{2\sqrt{3}}{13}} + 5x^{\sqrt{\frac{13}{14}}} + 4x^{\frac{1}{\sqrt{2}}} + 2x^{\frac{2}{\sqrt{11}}} + x^{\frac{1}{2}} + x^{\frac{2\sqrt{3}}{7}} + x^{\frac{2\sqrt{3}}{3\sqrt{5}}}$
G_{12}	8.0358	$x^{\frac{2\sqrt{2}}{3}} + x^{\frac{3}{\sqrt{10}}} + 7x^{\frac{1}{\sqrt{2}}} + x^{\frac{2\sqrt{2}}{\sqrt{21}}} + x^{\frac{1}{\sqrt{3}}}$

Table 2: Polynomials of ABC_3

Molecular graphs	ABC_4 Descriptor	ABC_4 polynomials
G_1	6.2722	$3x^{\sqrt{\frac{2}{5}}} + x^{\frac{\sqrt{7}}{3\sqrt{2}}} + 2x^{\frac{2\sqrt{2}}{5}} + 2x^{\frac{3}{\sqrt{30}}} + x^{\frac{\sqrt{11}}{2\sqrt{10}}} + 2x^{\frac{1}{2}}$
G_2	9.93131	$x^{\frac{1}{\sqrt{2}}} + 2x^{\sqrt{\frac{2}{5}}} + 2x^{\frac{2\sqrt{2}}{\sqrt{21}}} + x^{\frac{3}{2\sqrt{7}}} + x^{\frac{2\sqrt{2}}{5}} + 3x^{\sqrt{\frac{2}{7}}} + 3x^{\sqrt{\frac{11}{42}}}$ $+x^{\frac{1}{2}} + 2x^{\frac{2\sqrt{3}}{7}} + 2x^{\frac{\sqrt{13}}{2\sqrt{14}}}$
G_3	24.2177	$2x^{\frac{1}{\sqrt{2}}} + 3x^{\frac{\sqrt{7}}{3\sqrt{2}}} + x^{\frac{2\sqrt{2}}{\sqrt{21}}} + x^{\frac{3}{2\sqrt{6}}} + 2x^{\frac{\sqrt{6}}{4}} + 4x^{\frac{\sqrt{2}}{2\sqrt{5}}} + 2x^{\frac{1}{\sqrt{3}}} + x^{\frac{3}{2\sqrt{7}}}$ $+x^{\frac{\sqrt{11}}{6}} + 2x^{\frac{2\sqrt{2}}{5}} + 6x^{\frac{3}{\sqrt{30}}} + x^{\sqrt{\frac{10}{35}}} + 2x^{\frac{\sqrt{11}}{2\sqrt{10}}} + x^{\frac{2\sqrt{3}}{3\sqrt{6}}} + x^{\frac{\sqrt{10}}{6}}$ $+3x^{\sqrt{\frac{11}{42}}} + x^{\frac{1}{2}} + 4x^{\frac{2\sqrt{3}}{7}} + x^{\frac{\sqrt{13}}{2\sqrt{14}}} + x^{\frac{\sqrt{2}}{3}} + x^{\frac{\sqrt{14}}{8}} + 2x^{\frac{\sqrt{15}}{6\sqrt{2}}} + x^{\frac{4}{9}}$
G_4	24.4684	$2x^{\sqrt{\frac{2}{5}}} + 6x^{\frac{\sqrt{7}}{3\sqrt{2}}} + 2x^{\frac{2\sqrt{2}}{\sqrt{21}}} + 4x^{\frac{3}{\sqrt{30}}} + 6x^{\frac{\sqrt{10}}{6}} + 8x^{\sqrt{\frac{11}{42}}}$ $+10x^{\frac{1}{2}} + 3x^{\frac{\sqrt{13}}{2\sqrt{14}}} + 2x^{\frac{\sqrt{14}}{3\sqrt{7}}} + 2x^{\frac{\sqrt{14}}{8}} + x^{\frac{\sqrt{15}}{6\sqrt{2}}}$
G_5	13.1211	$2x^{\frac{1}{\sqrt{2}}} + 2x^{\sqrt{\frac{2}{5}}} + 4x^{\frac{\sqrt{7}}{2\sqrt{5}}} + 2x^{\frac{1}{\sqrt{3}}} + 3x^{\frac{2\sqrt{2}}{5}} + 3x^{\frac{3}{\sqrt{30}}}$ $+2x^{\sqrt{\frac{10}{35}}} + x^{\frac{\sqrt{11}}{2\sqrt{10}}} + 2x^{\sqrt{\frac{11}{42}}} + 2x^{\frac{\sqrt{13}}{2\sqrt{14}}}$
G_6	13.7239	$2x^{\frac{1}{\sqrt{2}}} + 3x^{\sqrt{\frac{2}{5}}} + 4x^{\frac{\sqrt{7}}{2\sqrt{5}}} + x^{\frac{1}{\sqrt{3}}} + 3x^{\frac{2\sqrt{2}}{5}} + 4x^{\frac{3}{\sqrt{30}}}$ $+2x^{\sqrt{\frac{10}{35}}} + x^{\frac{\sqrt{11}}{2\sqrt{10}}} + 2x^{\sqrt{\frac{11}{42}}} + 2x^{\frac{\sqrt{13}}{2\sqrt{14}}}$
G_7	27.6572	$3x^{\sqrt{\frac{2}{5}}} + 6x^{\frac{\sqrt{7}}{3\sqrt{2}}} + 5x^{\frac{\sqrt{6}}{4}} + 8x^{\frac{\sqrt{7}}{2\sqrt{5}}} + 2x^{\frac{2\sqrt{2}}{5}} + 7x^{\sqrt{\frac{3}{10}}} + 2x^{\frac{\sqrt{11}}{2\sqrt{10}}}$ $+x^{\sqrt{\frac{13}{45}}} + 7x^{\frac{\sqrt{10}}{6}} + 3x^{\sqrt{\frac{11}{42}}} + 3x^{\frac{1}{2}} + x^{\frac{\sqrt{13}}{3\sqrt{6}}} + x^{\frac{\sqrt{15}}{6\sqrt{2}}}$
G_8	17.1671	$x^{\frac{1}{\sqrt{2}}} + 2x^{\frac{\sqrt{5}}{2\sqrt{3}}} + x^{\sqrt{\frac{2}{5}}} + 2x^{\frac{\sqrt{7}}{3\sqrt{2}}} + 2x^{\frac{2\sqrt{2}}{21}} + 2x^{\frac{\sqrt{3}}{2\sqrt{2}}}$ $+2x^{\frac{\sqrt{7}}{2\sqrt{5}}} + x^{\frac{1}{\sqrt{3}}} + x^{\frac{2\sqrt{2}}{5}} + 4x^{\sqrt{\frac{3}{10}}} + x^{\frac{\sqrt{11}}{2\sqrt{10}}} + x^{\frac{\sqrt{5}}{3\sqrt{2}}}$ $+x^{\sqrt{\frac{11}{42}}} + 2x^{\frac{1}{2}} + x^{\frac{\sqrt{13}}{3\sqrt{6}}} + 3x^{\frac{\sqrt{13}}{2\sqrt{14}}} + 3x^{\frac{\sqrt{5}}{2\sqrt{6}}} + x^{\frac{4}{9}}$
G_9	29.9033	$5x^{\sqrt{\frac{2}{5}}} + 4x^{\frac{\sqrt{7}}{3\sqrt{2}}} + 5x^{\frac{\sqrt{6}}{4}} + 6x^{\frac{\sqrt{7}}{2\sqrt{5}}} + 3x^{\frac{2\sqrt{2}}{5}} + 10x^{\sqrt{\frac{3}{10}}}$ $+3x^{\frac{\sqrt{14}}{7}} + x^{\frac{\sqrt{11}}{2\sqrt{10}}} + 11x^{\frac{\sqrt{10}}{6}} + 3x^{\sqrt{\frac{11}{42}}} + 2x^{\frac{1}{2}}$
G_{10}	11.396	$x^{\sqrt{\frac{2}{5}}} + x^{\frac{\sqrt{7}}{3\sqrt{2}}} + 2x^{\frac{2\sqrt{2}}{\sqrt{21}}} + x^{\frac{\sqrt{3}}{2\sqrt{2}}} + 2x^{\frac{\sqrt{7}}{2\sqrt{5}}} + 2x^{\frac{2\sqrt{2}}{5}} + x^{\sqrt{\frac{3}{10}}}$ $+3x^{\sqrt{\frac{11}{10}}} + x^{\frac{\sqrt{10}}{6}} + x^{\frac{1}{2}} + 2x^{\frac{\sqrt{13}}{2\sqrt{14}}} + 2x^{\frac{\sqrt{3}}{3}} + x^{\frac{\sqrt{7}}{2\sqrt{8}}} + x^{\frac{\sqrt{5}}{2\sqrt{6}}}$
G_{11}	8.60999	$x^{\frac{1}{\sqrt{2}}} + 2x^{\sqrt{\frac{2}{5}}} + 2x^{\frac{\sqrt{7}}{3\sqrt{2}}} + 2x^{\frac{\sqrt{7}}{2\sqrt{5}}} + x^{\frac{1}{\sqrt{3}}} + x^{\sqrt{\frac{3}{10}}}$ $+x^{\sqrt{\frac{2}{7}}} + x^{\frac{\sqrt{11}}{2\sqrt{10}}} + 2x^{\sqrt{\frac{11}{42}}} + 2x^{\frac{1}{2}}$
G_{12}	6.60771	$x^{\frac{1}{\sqrt{2}}} + x^{\frac{\sqrt{5}}{2\sqrt{3}}} + 3x^{\frac{\sqrt{6}}{4}} + 3x^{\frac{\sqrt{7}}{2\sqrt{5}}} + 3x^{\sqrt{\frac{3}{10}}}$

Table 3: Polynomials of ABC_4

Molecular graphs	ABC_5 Descriptor	ABC_5 polynomials
G_1	6.76518	$x^{\frac{2}{3}} + 3x^{\frac{\sqrt{5}}{2\sqrt{3}}} + x^{\frac{\sqrt{6}}{4}} + 6x^{\frac{\sqrt{7}}{2\sqrt{5}}}$
G_2	9.98758	$x^{\frac{2\sqrt{2}}{5}} + 4x^{\frac{3}{\sqrt{30}}} + 6x^{\sqrt{\frac{13}{42}}} + 2x^{\frac{2\sqrt{3}}{7}} + 3x^{\frac{\sqrt{13}}{2\sqrt{14}}} + 3x^{\frac{\sqrt{17}}{3\sqrt{8}}}$
G_3	16.3041	$2x^{\frac{\sqrt{17}}{3\sqrt{10}}} + 4x^{\sqrt{\frac{19}{110}}} + 4x^{\frac{\sqrt{21}}{2\sqrt{33}}} + 7x^{\frac{\sqrt{23}}{2\sqrt{39}}} + x^{\frac{2\sqrt{6}}{13}} + 7x^{\frac{5}{\sqrt{182}}}$ $+5x^{\frac{3\sqrt{3}}{\sqrt{210}}} + 4x^{\frac{\sqrt{29}}{4\sqrt{15}}} + x^{\frac{\sqrt{30}}{16}} + 4x^{\frac{\sqrt{31}}{4\sqrt{17}}} + 5x^{\frac{\sqrt{33}}{3\sqrt{34}}}$
G_4	17.4374	$x^{\frac{\sqrt{14}}{8}} + 3x^{\frac{\sqrt{15}}{6\sqrt{2}}} + x^{\frac{4}{9}} + 7x^{\frac{\sqrt{17}}{3\sqrt{10}}} + x^{\frac{3\sqrt{2}}{10}} + 8x^{\sqrt{\frac{19}{110}}}$ $+6x^{\frac{\sqrt{21}}{2\sqrt{33}}} + x^{\sqrt{\frac{22}{143}}} + 6x^{\frac{\sqrt{23}}{2\sqrt{39}}} + 4x^{\frac{5}{\sqrt{182}}} + 5x^{\frac{3\sqrt{3}}{\sqrt{210}}}$
G_5	9.87346	$x^{\frac{2\sqrt{3}}{7}} + 3x^{\frac{\sqrt{13}}{2\sqrt{14}}} + 3x^{\frac{\sqrt{15}}{6\sqrt{2}}} + 4x^{\frac{\sqrt{17}}{3\sqrt{10}}} + 5x^{\sqrt{\frac{19}{110}}} + 4x^{\frac{\sqrt{21}}{2\sqrt{33}}} + 3x^{\frac{\sqrt{23}}{2\sqrt{39}}}$
G_6	9.99488	$3x^{\frac{\sqrt{13}}{2\sqrt{14}}} + 2x^{\frac{\sqrt{15}}{6\sqrt{2}}} + 3x^{\frac{\sqrt{17}}{3\sqrt{10}}} + 4x^{\sqrt{\frac{19}{110}}} + 6x^{\frac{\sqrt{21}}{2\sqrt{33}}} + 4x^{\frac{\sqrt{23}}{2\sqrt{39}}} + 2x^{\frac{5}{\sqrt{182}}}$
G_7	18.0119	$3x^{\frac{\sqrt{17}}{3\sqrt{10}}} + 3x^{\sqrt{\frac{19}{110}}} + 4x^{\frac{\sqrt{21}}{2\sqrt{33}}} + 6x^{\frac{\sqrt{23}}{2\sqrt{39}}} + 7x^{\frac{5}{\sqrt{182}}} + 7x^{\frac{3}{\sqrt{70}}}$ $+8x^{\frac{\sqrt{29}}{4\sqrt{15}}} + 7x^{\frac{\sqrt{31}}{4\sqrt{17}}} + 4x^{\sqrt{\frac{11}{103}}}$
G_8	13.8153	$3x^{\sqrt{\frac{11}{42}}} + 5x^{\frac{\sqrt{13}}{2\sqrt{14}}} + x^{\frac{\sqrt{14}}{8}} + 5x^{\frac{\sqrt{30}}{12}} + 6x^{\frac{\sqrt{17}}{3\sqrt{10}}} + x^{\frac{3\sqrt{2}}{10}} + 6x^{\sqrt{\frac{19}{110}}} + 4x^{\frac{\sqrt{21}}{2\sqrt{33}}}$
G_9	17.9476	$2x^{\frac{\sqrt{21}}{2\sqrt{33}}} + 4x^{\frac{\sqrt{23}}{2\sqrt{39}}} + 4x^{\frac{5}{\sqrt{182}}} + 7x^{\frac{3\sqrt{3}}{\sqrt{210}}} + 6x^{\frac{\sqrt{29}}{4\sqrt{15}}} + 6x^{\frac{\sqrt{31}}{4\sqrt{17}}} + 5x^{\sqrt{\frac{11}{103}}}$ $+5x^{\frac{\sqrt{35}}{3\sqrt{38}}} + 5x^{\frac{\sqrt{37}}{2\sqrt{95}}} + x^{\frac{\sqrt{38}}{20}} + 3x^{\frac{\sqrt{39}}{2\sqrt{105}}} + 4x^{\frac{\sqrt{41}}{\sqrt{462}}} + x^{\frac{\sqrt{42}}{22}}$
G_{10}	10.5748	$x^{\frac{2\sqrt{2}}{5}} + 4x^{\sqrt{\frac{3}{10}}} + 7x^{\sqrt{\frac{11}{42}}} + x^{\frac{2\sqrt{3}}{7}} + 4x^{\frac{\sqrt{13}}{2\sqrt{14}}} + 3x^{\frac{\sqrt{5}}{2\sqrt{6}}} + x^{\frac{4}{9}}$
G_{11}	8.21547	$x^{\frac{\sqrt{6}}{4}} + 3x^{\frac{\sqrt{7}}{2\sqrt{5}}} + 6x^{\sqrt{\frac{3}{10}}} + 4x^{\sqrt{\frac{11}{42}}} + x^{\frac{2\sqrt{3}}{7}}$
G_{12}	5.80712	$2x^{\frac{\sqrt{7}}{2\sqrt{5}}} + 3x^{\sqrt{\frac{3}{10}}} + 3x^{\sqrt{\frac{11}{42}}} + 3x^{\frac{\sqrt{13}}{2\sqrt{14}}}$

Table 4: Polynomials of ABC_5

Molecular graphs	ABC_6 Descriptor	ABC_6 polynomials
G_1	7.50714	$7x^{\frac{1}{\sqrt{2}}} + 2x^{\frac{2}{3}} + x^{\sqrt{\frac{2}{5}}} + x^{\frac{\sqrt{7}}{2\sqrt{5}}}$
G_2	11.7441	$7x^{\frac{1}{\sqrt{2}}} + x^{\frac{2}{3}} + 2x^{\frac{\sqrt{5}}{2\sqrt{3}}} + 5x^{\frac{\sqrt{6}}{4}} + 3x^{\frac{\sqrt{7}}{2\sqrt{5}}}$
G_3	28.8953	$17x^{\frac{1}{\sqrt{2}}} + 7x^{\frac{2}{3}} + 3x^{\frac{\sqrt{5}}{2\sqrt{3}}} + 8x^{\sqrt{\frac{2}{5}}} + x^{\frac{\sqrt{7}}{3\sqrt{2}}}$ $+x^{\frac{\sqrt{6}}{4}} + 2x^{\frac{\sqrt{7}}{2\sqrt{5}}} + 3x^{\frac{2\sqrt{2}}{5}} + 2x^{\frac{3}{\sqrt{30}}}$
G_4	29.4258	$14x^{\frac{1}{\sqrt{2}}} + 8x^{\frac{\sqrt{5}}{2\sqrt{3}}} + 4x^{\sqrt{\frac{2}{5}}} + 6x^{\frac{\sqrt{6}}{4}} + 9x^{\frac{\sqrt{7}}{2\sqrt{5}}}$ $+2x^{\frac{1}{\sqrt{3}}} + 2x^{\frac{2\sqrt{2}}{5}} + x^{\frac{3}{\sqrt{30}}}$
G_5	15.5026	$13x^{\frac{1}{\sqrt{2}}} + 2x^{\frac{2}{3}} + 3x^{\frac{\sqrt{5}}{2\sqrt{3}}} + x^{\sqrt{\frac{2}{5}}} + 2x^{\frac{\sqrt{6}}{4}} + 2x^{\frac{\sqrt{7}}{2\sqrt{5}}}$
G_6	16.612	$1 + 12x^{\frac{1}{\sqrt{2}}} + x^{\sqrt{\frac{2}{3}}} + 2x^{\frac{2}{3}} + 3x^{\frac{\sqrt{5}}{2\sqrt{3}}}$ $+x^{\sqrt{\frac{2}{5}}} + 2x^{\frac{\sqrt{6}}{4}} + 2x^{\frac{\sqrt{7}}{2\sqrt{5}}}$
G_7	33.0262	$24x^{\frac{1}{\sqrt{2}}} + 8x^{\frac{2}{3}} + 8x^{\frac{\sqrt{5}}{2\sqrt{3}}} + 5x^{\sqrt{\frac{2}{5}}}$ $+x^{\frac{\sqrt{7}}{3\sqrt{2}}} + 2x^{\frac{\sqrt{6}}{4}} + x^{\sqrt{\frac{3}{10}}}$
G_8	20.7622	$1 + 10x^{\frac{1}{\sqrt{2}}} + x^{\sqrt{\frac{2}{3}}} + x^{\frac{\sqrt{3}}{2}} + 5x^{\frac{2}{3}} + 2x^{\frac{\sqrt{5}}{2\sqrt{3}}} + x^{\sqrt{\frac{2}{5}}}$ $+x^{\frac{\sqrt{7}}{3\sqrt{2}}} + 5x^{\frac{\sqrt{7}}{2\sqrt{5}}} + 3x^{\sqrt{\frac{3}{10}}} + x^{\frac{\sqrt{10}}{6}}$
G_9	35.8108	$24x^{\frac{1}{\sqrt{2}}} + 12x^{\frac{2}{3}} + 13x^{\frac{\sqrt{5}}{2\sqrt{3}}} + x^{\sqrt{\frac{2}{5}}} + 2x^{\frac{\sqrt{6}}{4}} + x^{\frac{\sqrt{7}}{2\sqrt{5}}}$
G_{10}	13.6573	$9x^{\frac{1}{\sqrt{2}}} + x^{\frac{2}{3}} + x^{\frac{\sqrt{5}}{2\sqrt{3}}} + 4x^{\sqrt{\frac{2}{5}}} + 2x^{\frac{\sqrt{7}}{2\sqrt{5}}}$ $+2x^{\frac{1}{\sqrt{3}}} + x^{\frac{2\sqrt{2}}{5}} + x^{\sqrt{\frac{3}{10}}}$
G_{11}	10.1919	$9x^{\frac{1}{\sqrt{2}}} + x^{\frac{2}{3}} + 3x^{\frac{\sqrt{5}}{2\sqrt{3}}} + 2x^{\frac{\sqrt{6}}{4}}$
G_{12}	7.94975	$1 + 7x^{\frac{1}{\sqrt{2}}} + 3x^{\frac{2}{3}}$

Table 5: Polynomials of ABC_6

Quantitative Data Set
The efficiency of these molecular descriptors was examined utilizing the data set of these drugs are listed in Table 6., found at [1, 32–35, 52]. The data set comprises of the subsequent information: Molecular weight (MW), Topological polar surface: The polar surface area (PSA) or topological polar surface area ($TPSA$) of a particle is characterized as the surface aggregate over every polar molecule, fundamentally oxygen and nitrogen, additionally including their joined hydrogen molecules. The Binding energy (BE): Binding energy, a measure of energy needed to isolate a molecule from an arrangement of particles or to scatter all of the particles of the framework. Binding energy is particularly material to subatomic particles in nuclear cores, to electrons bound to nuclei in molecules, and to nuclei and particles bound together in crystals. The $xlogP3$: $xlogP3$ predicts the $logP$ estimation of a query compound by utilizing the known $logP$ estimation of a reference compound as a beginning stage. The distinction in the $logP$ estimations of the inquiry compound and the reference compound is then assessed by an added substance model. All these values are mentioned in Table 6.

Compound Name	Molecular weight	Topological polar surface area	Binding energy	$XlogP3$
Ritonovir	720.9	202	−10.6	6
Lopinavir	628.8	120	−10.6	5.9
Arbidol	477.4	80	−11.5	4.4
Thalidomide	258.23	83.6	−7.17	0.3
2-phenoxyethanol	138.16	29.5	−5.76	1.2
Histadine	155.15	92	−77.43	-3.2
Favipiravir	157.1	84.6	−5.4	-0.6
Ribavirin	244.2	144.0	−5.6	-1.8
Remdesivir	602.58	213.36	−6.3	1.9
Theaflavin	564.49	218.0$	−9.6	2.4
Chloroquine	319.9	28.2	−5.1	4.6
Hydroxychloroquine	335.9	48.4	−5.3	3.6

Table 6: Quantitative properties of molecular structures

5 Analysis and Discussion

In this section, statistical regression analysis has been done by using linear model $y = A + Bx$, nonlinear model $y = A + Bx + Cx^2$. Here y be the required property of the drug, x be the topological indices and A, B, C are constants. The regression models were applied to the properties and ABC_i indices mentioned in Tables [1-5].

5.1 Linear and nonlinear regression models of ABC indices

Linear model for Molecular weights (MW) of the drugs and ABC_i indices.

$$MW_1 = 52.98473 + 13.11706(ABC_1)$$
$$MW_2 = 34.6026 + 15.15078(ABC_2)$$
$$MW_3 = 30.91389 + 16.08657(ABC_3)$$
$$MW_4 = 52.21115 + 16.94347(ABC_4)$$
$$MW_5 = -42.24596 + 30.43402(ABC_5)$$
$$MW_6 = 52.49117 + 14.14205(ABC_6)$$

Nonlinear model for Molecular weights (MW) of the drugs and ABC_i indices

$$MW_7 = 49.02522 + 13.56222(ABC_1) - 0.00973(ABC_1)^2$$
$$MW_8 = 57.75665 + 12.59312(ABC_2) + 0.05711(ABC_2)^2$$
$$MW_9 = -68.74416 + 28.15147(ABC_3) - 0.30117(ABC_3)^2$$
$$MW_{10} = 6.66753 + 23.43809(ABC_4) - 0.18208(ABC_4)^2$$
$$MW_{11} = -87.16106 + 38.612(ABC_5) - 0.32836(ABC_5)^2$$
$$MW_{12} = 14.52369 + 18.67716(ABC_6) - 0.10637(ABC_6)^2$$

From the Table 7, one can observe that R^2 values 0.11131, 0.10067, and

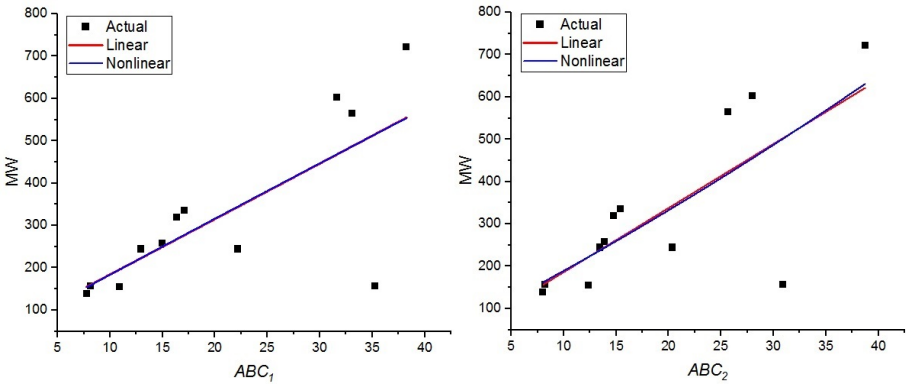

Figure 3: Plots of MW Vs ABC_1 and ABC_2

0.13105 of models MW_1, MW_6 and, MW_7, and R^2 values 0.56288 and 0.50097 of MW_9, MW_{12} respectively, are well correlated. Further, we discuss the regression models for the topological polar surface area ($TPSA$) of chemical drugs mentioned in Table [1-5]. ABC_i indices.

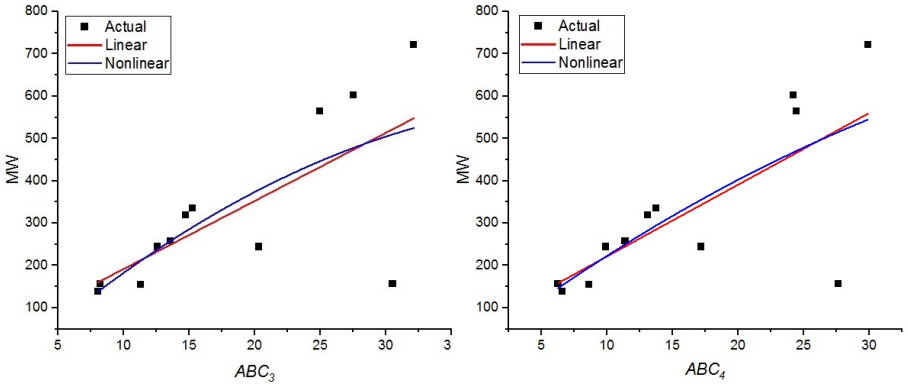

Figure 4: Plots of MW Vs ABC_3 and ABC_4

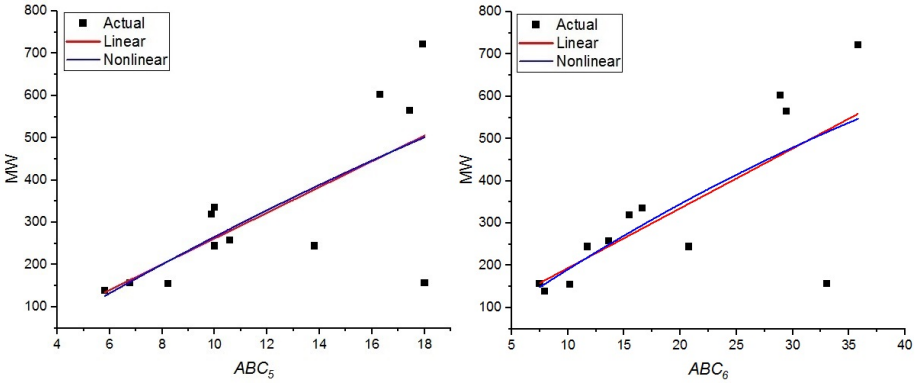

Figure 5: Plots of MW Vs ABC_5 and ABC_6

Model number	R^2 values	F values	Significance F values
MW_1	0.11131	2.37776	0.1541
MW_2	0.06069	1.71072	0.22016
MW_3	0.07598	1.90454	0.19764
MW_4	-0.09875	0.01141	0.91705
MW_5	-0.01927	0.79199	0.39441
MW_6	0.10067	2.23139	0.1661
MW_7	0.13105	1.82948	0.21543
MW_8	0.42653	5.09072	0.0332
MW_9	0.56288	8.08222	0.00978
MW_{10}	-0.22017	0.00756	0.99247
MW_{11}	0.44761	5.45667	0.02805
MW_{12}	0.50097	6.52137	0.01776

Table 7: Statistical values for Molecular weight and ABC_i indices.

Linear model for $TPSA$ of the drugs and ABC_i indices.

$$
\begin{aligned}
TPSA_1 &= 16.35464 + 4.61378(ABC_1)\\
TPSA_2 &= 12.50325 + 5.19264(ABC_2)\\
TPSA_3 &= 7.16695 + 5.73624(ABC_3)\\
TPSA_4 &= 17.9612 + 5.84291(ABC_4)\\
TPSA_5 &= -29.38536 + 11.71995(ABC_5)\\
TPSA_6 &= 18.29508 + 4.86452(ABC_6)
\end{aligned}
$$

Nonlinear model for $TPSA$ of the drugs and ABC_i indices.

$$
\begin{aligned}
TPSA_7 &= 71.67944 - 1.60629(ABC_1) + 0.184(ABC_1)^2\\
TPSA_8 &= -3.8892 + 7.0034(ABC_2) - 0.04044(ABC_2)^2\\
TPSA_9 &= 28.97766 + 3.09577(ABC_3) + 0.06591(ABC_3)^2\\
TPSA_{10} &= 54.31515 - 3.51994(ABC_4) + 0.09582(ABC_4)^2\\
TPSA_{11} &= -59.41646 + 21.50948(ABC_5) + 0.61192(ABC_5)^2\\
TPSA_{12} &= 67.55793 - 1.01979(ABC_6) + 0.13801(ABC_6)^2
\end{aligned}
$$

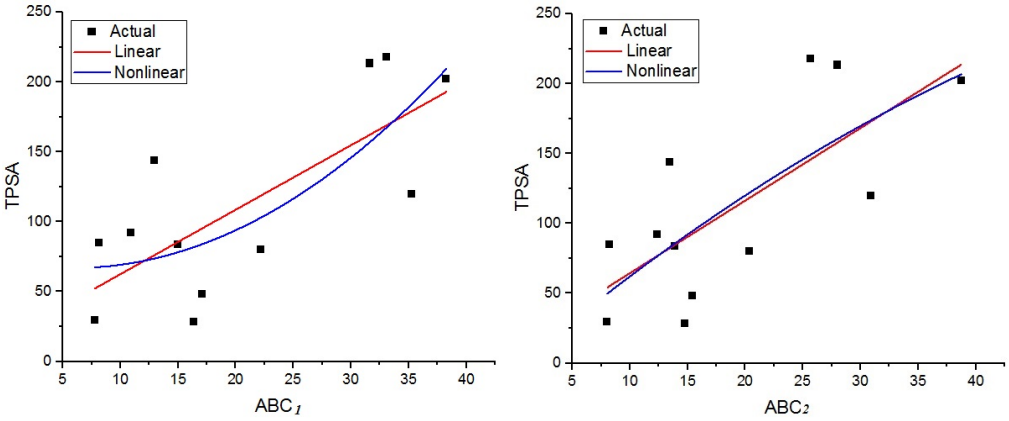

Figure 6: Plots of $TPSA$ Vs ABC_1 and ABC_2

From the Table 8, one can observe that R^2 values of the models $TPSA_1$ to $TPSA_{12}$ is between 0.4 and 0.55 and are well correlated. Further, we discuss the regression models for binding energy (BE) of chemical drugs.

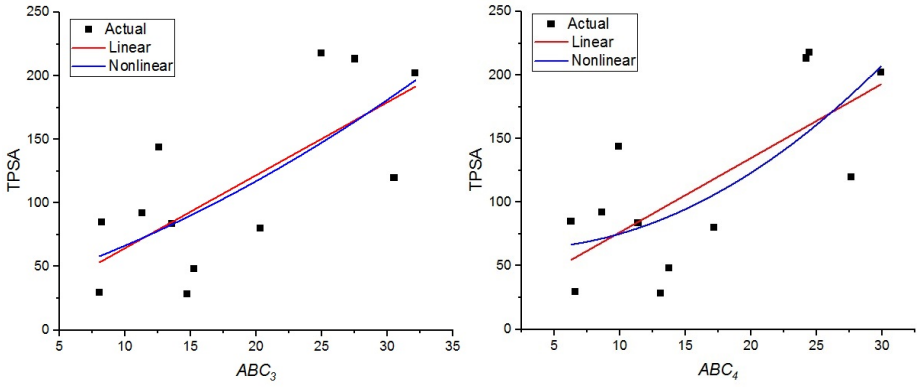

Figure 7: Plots of $TPSA$ Vs ABC_3 and ABC_4

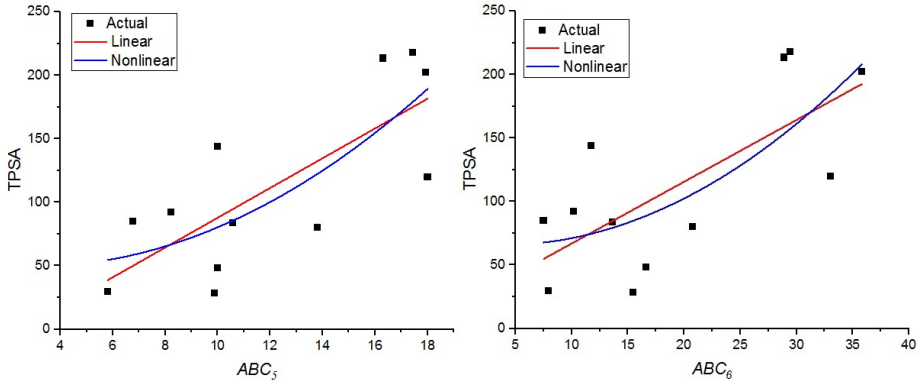

Figure 8: Plots of $TPSA$ Vs ABC_5 and ABC_6

Linear model for BE values of the drugs and ABC_i indices.

$$BE_1 = 7.09528 - 0.08249(ABC_1)$$
$$BE_2 = 4.69748 + 0.05691(ABC_2)$$
$$BE_3 = 7.48664 - 0.11579(ABC_3)$$
$$BE_4 = 6.89543 - 0.09228(ABC_4)$$
$$BE_5 = 8.15575 - 0.16133(ABC_5)$$
$$BE_6 = 7.76587 - 0.10259(ABC_6)$$

Model number	R^2 values	F values	Significance F values
$TPSA_1$	0.50766	12.34231	0.0056
$TPSA_2$	0.49016	11.57558	0.00675
$TPSA_3$	0.46622	10.60791	0.00862
$TPSA_4$	0.46721	10.64602	0.00853
$TPSA_5$	0.53763	13.79052	0.00402
$TPSA_6$	0.46509	10.56413	0.00872
$TPSA_7$	0.48369	6.15257	0.0207
$TPSA_8$	0.43651	5.26059	0.03068
$TPSA_9$	0.41	4.82203	0.03773
$TPSA_{10}$	0.42899	5.13214	0.03256
$TPSA_{11}$	0.5053	6.61794	0.01707
$TPSA_{12}$	0.42983	5.14633	0.03235

Table 8: Statistical values for $TPSA$ and ABC_i indices

Nonlinear model for Binding energy (BE) of the drugs and ABC_i indices.

$$BE_7 = 7.18181 - 0.261227(ABC_1) - 0.02116(ABC_1)^2$$
$$BE_8 = -3.15561 - 0.24398(ABC_2) + 0.00796(ABC_2)^2$$
$$BE_9 = 2.47063 + 0.5299(ABC_3) - 0.01692(ABC_3)^2$$
$$BE_{10} = 1.90712 + 0.68861(ABC_4) - 0.02104(ABC_4)^2$$
$$BE_{11} = 6.7491 + 0.01759(ABC_5) - 0.00427(ABC_5)^2$$
$$BE_{12} = 2.66625 + 0.40248(ABC_6) - 0.01032(ABC_6)^2$$

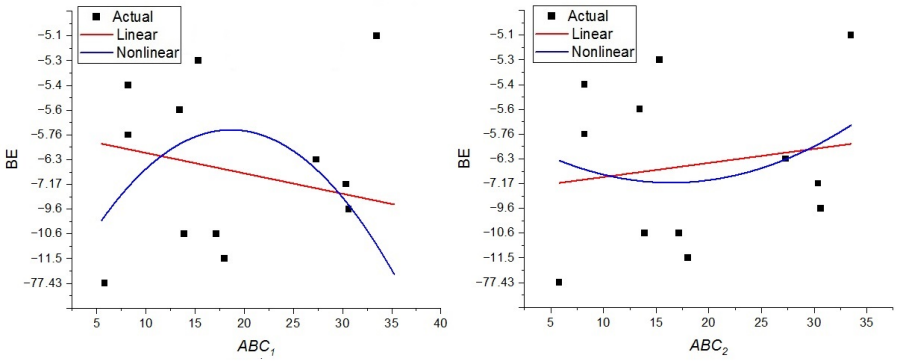

Figure 9: Plots of BE Vs ABC_1 and ABC_2

From the Table 9, one can observe that R^2 values 0.11766, 0.13955, and 0.27119 of models BE_5, BE_7, and BE_{11} respectively, are well correlated.

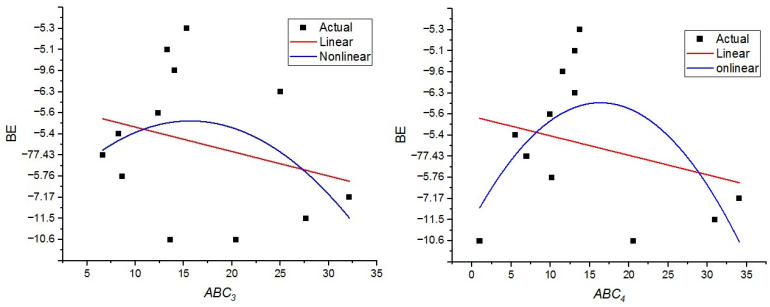

Figure 10: Plots of BE Vs ABC_3 and ABC_4

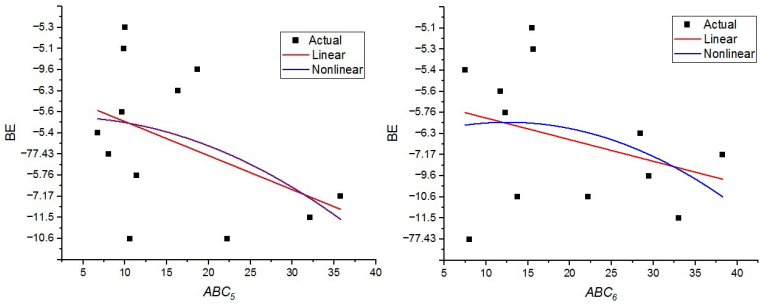

Figure 11: Plots of BE Vs ABC_5 and ABC_6

Model number	R^2 values	F values	Significance F values
BE_1	-0.052	0.45622	0.51471
BE_2	-0.06921	0.28795	0.60327
BE_3	-0.01919	0.79292	0.39414
BE_4	-0.02524	0.72919	0.41313
BE_5	0.11766	2.46691	0.14734
BE_6	-0.07081	0.27262	0.61295
BE_7	0.13955	1.89203	0.2061
BE_8	-0.15424	0.26505	0.77295
BE_9	0.01458	1.16279	0.30621
BE_{10}	-0.03834	0.7969	0.48013
BE_{11}	0.27119	3.04654	0.09763
BE_{12}	-0.11951	0.41288	0.67366

Table 9: Statistical values for BE and ABC_i indices

Linear model for $xlogp3$ values of the drugs and ABC_i indices.

$$xlogP3_1 = -1.82079 + 0.18718(ABC_1)$$
$$xlogP3_2 = -1.94823 + 0.20916(ABC_2)$$
$$xlogP3_3 = -2.37821 + 0.24282(ABC_3)$$
$$xlogP3_4 = 1.34229 + 0.05036(ABC_4)$$
$$xlogP3_5 = -2.02011 + 0.25348(ABC_5)$$
$$xlogP3_6 = -3.09041 + 0.42688(ABC_6)$$

Nonlinear model for $xlogp3$ values of the drugs and ABC_i indices

$$xlogP3_7 = -3.59233 + 0.38635(ABC_1)) - 0.00436(ABC_1)^2$$
$$xlogP3_8 = -2.52282 + 0.27263(ABC_2) - 0.00142(ABC_2)^2$$
$$xlogP3_9 = -3.14533 + 0.33569(ABC_3) - 0.00232(ABC_3)^2$$
$$xlogP3_{10} = -3.81685 + 0.5097(ABC_4) - 0.00718(ABC_4)^2$$
$$xlogP3_{11} = -1.40031 + 0.11916(ABC_5) + 0.01236(ABC_5)^2$$
$$xlogP3_{12} = -3.89001 + 0.43466(ABC_6) - 0.00522(ABC_6)^2$$

From the Table 10, one can observe that R^2 values 0.4251, 0.40273, 0.43273,

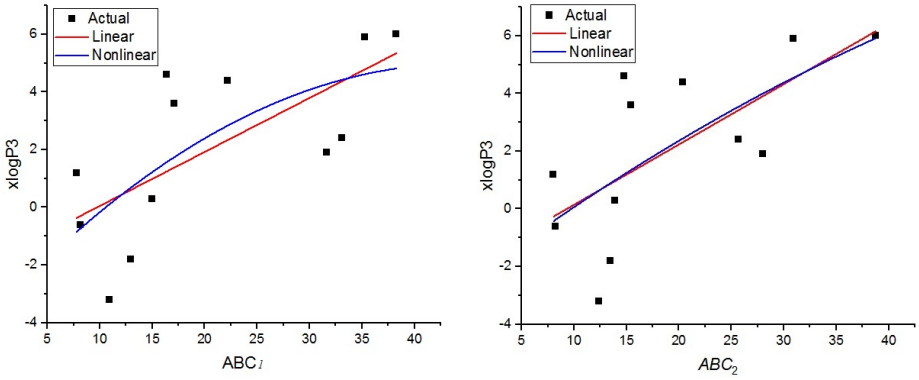

Figure 12: Plots of $xlogp3$ Vs ABC_1 and ABC_2

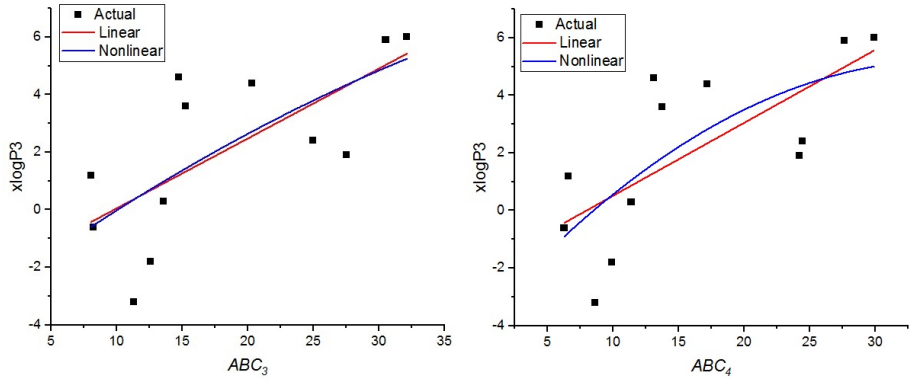

Figure 13: Plots of $xlogp3$ Vs ABC_3 and ABC_4

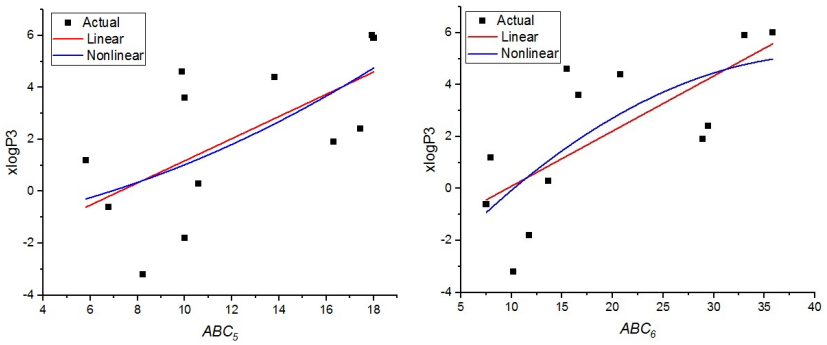

Figure 14: Plots of $xlogp3$ Vs ABC_5 and ABC_6

Model number	R^2 values	F values	Significance F values
$xlogP3_1$	0.4251	9.13392	0.01285
$xlogP3_2$	0.40273	8.41713	0.0158
$xlogP3_3$	0.43273	9.39104	0.01195
$xlogP3_4$	0.46049	10.38897	0.00913
$xlogP3_5$	0.34415	6.77201	0.02639
$xlogP3_6$	0.46434	10.53551	0.00878
$xlogP3_7$	0.37777	4.33923	0.04793
$xlogP3_8$	0.3383	3.81189	0.06321
$xlogP3_9$	0.3717	4.25378	0.05007
$xlogP3_{10}$	0.41734	4.93945	0.03566
$xlogP3_{11}$	0.27535	3.08987	0.09515
$xlogP3_{12}$	0.42298	5.03171	0.03413

Table 10: Statistical values for $xlogp3$ and ABC_i indices.

0.41734 and 0.42298 of models $xlogP3_1$, $xlogP3_2$, $xlogP3_3$, $xlogP3_{10}$ and , $xlogP3_{12}$ and R^2 values 0.46049 and 0.46434 of $xlogP3_4$ and $xlogP3_6$ respectively, are well correlated.

5.2 Inference of ABC polynomials

we have analyzed the ABC indices and their polynomials to the respective graphs. The plotting has been done by using Origin software and obtained the R^2 values, F values, and significance F values. From plotting of these polynomials, we obtained the R^2 and F values, which are tabulated in Table 11. (a) and (b), Table 12. (c) and (d), and Table 13. (e) and (f). These Tables shows that the R^2 values of the respective plots are between 0.9 and 1. Hence, they are good fit and have a strong correlation.

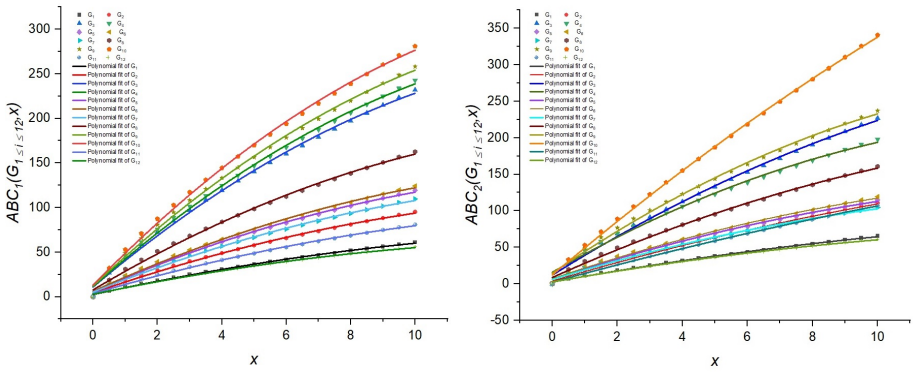

Figure 15: Plots of $ABC_1(G_{1\leq i\leq 12})$ and $ABC_2(G_{1\leq i\leq 12})$ Vs Molecular graphs

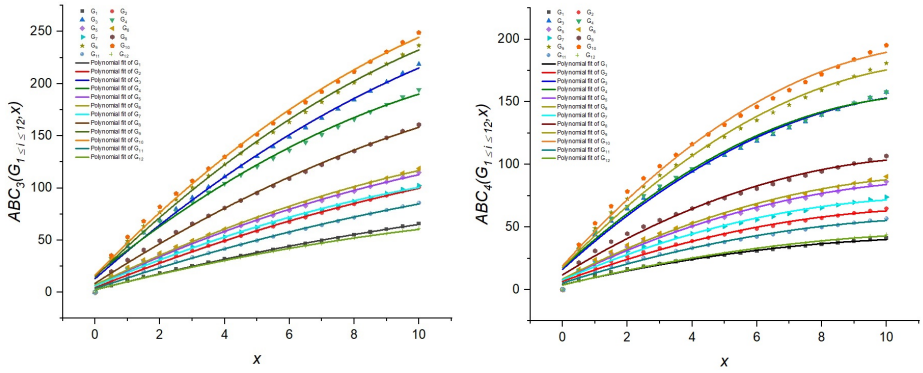

Figure 16: Plots of $ABC_3(G_{1\leq i\leq 12})$ and $ABC_4(G_{1\leq i\leq 12})$ Vs Molecular graphs

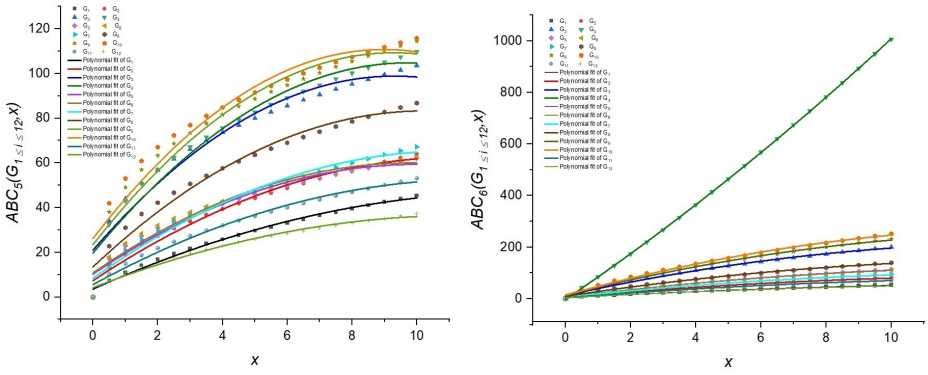

Figure 17: Plots of $ABC_5(G_{1\leq i\leq 12})$ and $ABC_6(G_{1\leq i\leq 12})$ Vs Molecular graphs

Graphs	R^2 values	F values
G1	0.99782	4568.75898
G2	0.99726	3646.51741
G3	0.99721	3572.00533
G4	0.99722	3583.58904
G5	0.99699	3310.31343
G6	0.99698	3299.84643
G7	0.99708	3418.49128
G8	0.99715	3494.32749
G9	0.99721	3572.46354
G10	0.99729	3676.7526
G11	0.9975	3992.22619
G12	0.99675	3065.13793

(a)

Graphs	R^2 values	F values
G1	0.99839	6187.73986
G2	0.99861	7186.47307
G3	0.99685	3162.31656
G4	0.99234	1296.5373
G5	0.99602	2501.76792
G6	0.99597	2471.70221
G7	0.99613	2577.5748
G8	0.99666	2989.42182
G9	0.9955	2215.60131
G10	0.9989	9068.26869
G11	0.99949	19562.57086
G12	0.99779	4522.62154

(b)

Table 11: (a) Regression values of $ABC_1(G_i, x)$. (b) Regression values of $ABC_2(G_i, x)$; where $1 \leq i \leq 12$

Graphs	R^2 values	F values
G1	0.99844	6413.1
G2	0.99772	4384.96
G3	0.99584	2395.98
G4	0.99166	1190.69
G5	0.99599	2482.86
G6	0.99585	2402.26
G7	0.9957	2318.46
G8	0.99664	2963.86
G9	0.99545	2186.8
G10	0.99481	1918.94
G11	0.99795	4872.74
G12	0.9978	4538.44

(c)

Graphs	R^2 values	F values
G1	0.9882	840.366
G2	0.98637	724.87
G3	0.98617	713.87
G4	0.98369	604.07
G5	0.98835	849.21
G6	0.98849	859.68
G7	0.98517	665.47
G8	0.98382	609.11
G9	0.98758	796.18
G10	0.98751	791.82
G11	0.98873	877.97
G12	0.99099	1100.92

(d)

Table 12: (c) Regression values of $ABC_3(G_i, x)$. (d) Regression values of $ABC_4(G_i, x)$; where $1 \leq i \leq 12$

Graphs	R^2 values	F values
G1	0.992	1240.92
G2	0.98254	563.9
G3	0.93907	155.11
G4	0.95369	206.91
G5	0.96169	252.03
G6	0.9576	226.83
G7	0.97902	467.558
G8	0.9664	288.5873
G9	0.93759	151.23
G10	0.92182	118.91
G11	0.98553	682.09
G12	0.98293	576.78

(e)

Graphs	R^2 values	F values
G1	0.99585	2401.82
G2	0.99446	1795.02
G3	0.99469	1875.0
G4	0.99998	408991.67
G5	0.99556	2241.892
G6	0.99574	2340.56
G7	0.99439	1773.17
G8	0.99496	1976.18
G9	0.99548	2203.71
G10	0.99554	2233.23
G11	0.99572	2327.01
G12	0.99632	2705.26

(f)

Table 13: (e) Regression values of $ABC_5(G_i, x)$. (f) Regression values of $ABC_6(G_i, x)$; where $1 \leq i \leq 12$

6 Conclusion

The properties of molecular graphs of the chemical structures are important for the accomplishment of a new drug and can be distinguished from the study of topological indices, Favipiravir, Ribavirin, Remdesiver, Theaflavin, Chloroquine, Hydroxychloroquine, Lopinavir, Ritonavir, Arbidol, Thalidomide, Histidine, and 2-Phenoxyethanol are studied in this article, and established the valency, distance, neighborhood, eccentricity, and 2-distance based bond partitions for ABC (Atom bond connectivity) polynomials of these drugs. Further, the statistical analysis shows that different ABC polynomials figured in this article have solid prescient capacity for physicochemical properties of antiviral drugs. Nonetheless, the statistical analysis demonstrates that the R^2 values shows a strong correlation. The hypothetical results got in this article have significance in planning new drug and immunization for the treatment of COVID-19.

Conflict of Interests The authors declare that there is no conflict of interests regarding the publication of this article.

References

[1] Arshad, Usman, Henry Pertinez, Helen Box, Lee Tatham, Rajith KR Rajoli, Paul Curley, Megan Neary et al. Prioritisation of Anti-SARS-Cov-2 Drug Repurposing Opportunities Based on Plasma and Target Site Concentrations Derived from their Established Human Pharmacokinetics. Clinical Pharmacology & Therapeutics (2020).

[2] Wang, Manli, Ruiyuan Cao, Leike Zhang, Xinglou Yang, Jia Liu, Mingyue Xu, Zhengli Shi, Zhihong Hu, Wu Zhong, and Gengfu Xiao. Remdesivir and chloroquine effectively inhibit the recently emerged novel coronavirus (2019-nCoV) in vitro. Cell research 30, no. 3 (2020): 269-271.

[3] Zhou, Dan, Sheng-Ming Dai, and Qiang Tong. COVID-19: a recommendation to examine the effect of hydroxychloroquine in preventing infection and progression. Journal of Antimicrobial Chemotherapy (2020).

[4] Liu, Wenshe, Jared S. Morse, Tyler Lalonde, and Shiqing Xu. Learning from the past: possible urgent prevention and treatment options for severe acute respiratory infections caused by 2019-nCoV. Chembiochem (2020).

[5] Chaluvaraju, B., and Ameer Basha Shaikh. "Different Versions of Atom-Bond Connectivity Indices of Some Molecular Structures: Applied for the Treatment and Prevention of COVID-19." Polycyclic Aromatic Compounds (2021): 1-15.

[6] R. Todeschini and V. Consonni, Molecular Descriptors for Chemoinformatics, Wiley–VCH, Weinheim (2009).

[7] F. Harary, *Graph Theory*, Addison Wesley, *Reading Mass*, (1969).

[8] I. Gutman and O. E. Polansky, Mathematical Concepts in Organic Chemistry, Springer, Berlin (1986).

[9] Trinajstic, Nenad. Chemical graph theory. Routledge, (2018).

[10] I. Gutman, Degree–based topological indices, Croat. Chem. Acta. **86** (2013), 351–361.

[11] B. Chaluvaraju, H. S. Boregowda and I. N. Cangul, Some Inequalities for the First General Zagreb Index of Graphs and Line Graphs. Proc. Natl. Acad. Sci., India, Sect. A Phys. Sci. (2020): 1-10.

[12] Kulli, V. R., B. Chaluvaraju, and H. S. Boregowda. "The product connectivity Banhatti index of a graph." Discussiones Mathematicae Graph Theory 39, no. 2 (2019): 505-517.

[13] Kulli, V. R., B. Chaluvaraju, and H. S. Boregowda. "Some bounds on sum connectivity Banhatti index of graphs." Palestine Journal of Mathematics 8, no. 2 (2019): 355-364.

[14] I. Gutman, V. R. Kulli, B. Chaluvaraju and H. S. Boregowda, On Banhatti and Zagreb Indices. J. Int. Math. Virtual Inst. **7** (2017), 53–67.

[15] I. Gutman and N. Trinajstić, Graph Theory and molecular orbitals. Total π-electron energy of alternant hydrocarbons, Chem. Phys. Lett. **17** (1972), 535–538.

[16] V.R.Kulli, B. Chaluvaraju and T.V. Asha, Multiplicative product and sum connectivity indices of chemical structures in drugs, Research Review International Journal of Multidisciplinary, 4(2), (2019), 949–953.

[17] V.R. Kulli, K Banhatti indices of chloroquine and hydroxychloroquine: Research applied for the treatment and prevention of COVID-19, International Journal of Applied Chemistry, 7(1), (2019), 63–68.

[18] Mondal, Sourav, Nilanjan De, and Anita Pal. "Topological Indices of Some Chemical Structures Applied for the Treatment of COVID-19 Patients." Polycyclic Aromatic Compounds (2020), 1–15.

[19] Gao, Wei, and Weifan Wang. "Second atom-bond connectivity index of special chemical molecular structures." Journal of Chemistry (2014).

[20] Gao, Wei, et al. "The first multiplication atom-bond connectivity index of molecular structures in drugs." Saudi Pharmaceutical Journal 25.4 (2017), 548–555.

[21] Zheng, Lina, Yiqiao Wang, and Wei Gao. "Topological Indices of Hyaluronic Acid-Paclitaxel Conjugates' Molecular Structure in Cancer Treatment." Open Chemistry 17, no. 1 (2019): 81-87.

[22] Ali, Parvez, Syed Ajaz K. Kirmani, Osamah Al Rugaie, and Faizul Azam. "Degree-based topological indices and polynomials of hyaluronic acid-curcumin conjugates." Saudi Pharmaceutical Journal 28, no. 9 (2020): 1093-1100.

[23] Kirmani, Syed Ajaz K., Parvez Ali, and Faizul Azam. "Topological indices and QSPR/QSAR analysis of some antiviral drugs being investigated for the treatment of COVID-19 patients." International Journal of Quantum Chemistry (2020): e26594.

[24] Liu, Jia-Bao, Micheal Arockiaraj, M. Arulperumjothi, and Savari Prabhu. "Distance based and bond additive topological indices of certain repurposed antiviral drug compounds tested for treating COVID-19." International Journal of Quantum Chemistry (2021): e26617.

[25] E. Estrada, L. Torres, L. Rodriguez and I. Gutman, An atom-bond connectivity index: Modelling the enthalphy of formation of alkanes, Indian J. Chem. 37A (1998)849-855.

[26] Graovac and M. Ghorbani, A new version of atom–bond connectivity index, Acta Chim. Slov., 57 (2010) 609–612.

[27] M.R. Farahani, Computing a New Version of Atom-Bond Connectivity Index of Circumcoronene Series of Benzenoid Hk by Using Cut Method, Journal of Mathematical Nanoscience, 2(1), (2012) 15-20.

[28] M. Ghorbani and M.A. Hosseinzadeh, Computing ABC4 index of nanostar dendrimers, Optoelectron. Adv. Mater. – Rapid Commun., 4(9), (2010) 1419–1422.

[29] M. R. Farahani, Eccentricity version of atom-bond connectivity index of Benzenoid family ABC5(Hk), World Applied Sciences Journal,21 (9) (2013) 1260–1265.

[30] V. R. Kulli, Product Connectivity Leap Index and ABC Leap Index of Helm Graphs, Annals of Pure and Applied Mathematics, 18(2), (2018), 189–192.

[31] Cao B, Wang Y, Wen D, Liu W, Wang J, Fan G, Ruan L, Song B, Cai Y, Wei M, Li X, Xia J, Chen N, Xiang J, Yu T, Bai T, Xie X, Zhang L, Li C, Yuan Y, Chen H, Li H, Huang H, Tu S, Gong F, Liu Y, Wei Y, Dong C, Zhou F, Gu X, Xu J, Liu Z, Zhang Y, Li H, Shang L, Wang K, Li K, Zhou X, Dong X, Qu Z, Lu S, Hu X, Ruan S, Luo S, Wu J, Peng L, Cheng F, Pan L, Zou J, Jia C, Wang J, Liu X, Wang S, Wu X, Ge Q, He J, Zhan H, Qiu F, Guo L, Huang C, Jaki T, Hayden FG, Horby PW, Zhang D, Wang C. A Trial of Lopinavir-Ritonavir in Adults Hospitalized with Severe Covid-19. N Engl J Med. doi: 10.1056/NEJMoa2001282. Epub 2020 Mar 18. PMID: 32187464; PMCID: PMC7121492, (2020):382(19):1787-1799.

[32] Kumar, Yogesh, Harvijay Singh, and Chirag N. Patel. "In silico prediction of potential inhibitors for the main protease of SARS-CoV-2 using molecular docking and dynamics simulation based drug-repurposing." Journal of infection and public health 13, no. 9 (2020): 1210-1223.

[33] Padhi, Aditya, Aniruddha Seal, and Timir Tripathi. "How does arbidol inhibit the novel coronavirus SARS-CoV-2? atomistic insights from molecular dynamics simulations." (2020).

[34] Wang, Chen-Xi, Min Pu, Pei-Huan Zhang, Yang Gao, Zuo-Yin Yang, and Ming Lei. "Structure Simulation and Host–Guest Interaction of Histidine-Intercalated Hydrotalcite–Montmorillonite Complex." Minerals 8, no. 5 (2018): 198.

[35] Graves, Alan P., Devleena M. Shivakumar, Sarah E. Boyce, Matthew P. Jacobson, David A. Case, and Brian K. Shoichet. "Rescoring docking hit lists for model cavity sites: predictions and experimental testing." Journal of molecular biology 377, no. 3 (2008): 914-934.

[36] Rajendran DK, Rajagopal V, Alagumanian S, Santhosh Kumar T, Sathiya Prabhakaran SP, Kasilingam D. Systematic literature review on novel corona virus SARS-CoV-2: a threat to human era. Virusdisease, doi: 10.1007/s13337-020-00604-z. Epub 2020 Jun 11. PMID: 32656310; PMCID: PMC7288266, (2020);31(2):161-173.

[37] Schein, Catherine H. "Repurposing approved drugs for cancer therapy." British Medical Bulletin (2021).

[38] Crommelin DJA, Volkin DB, Hoogendoorn KH, Lubiniecki AS, Jiskoot W. The Science is There: Key Considerations for Stabilizing Viral Vector-Based Covid-19 Vaccines. J Pharm Sci., doi: 10.1016/j.xphs.2020.11.015. Epub 2020 Nov 23. PMID: 33242452; PMCID: PMC7682479., (2021) ;110(2):627-634.

[39] Heidary, Noushin, and David E. Cohen. "Hypersensitivity reactions to vaccine components." Dermatitis 16, no. 3 (2005): 115-120.

[40] Y. Furuta, B.B. Gowen, K. Takahashi, K. Shiraki, D.F.Smee, D. L. Barnard, Favipiravir (T-705), a novel viral RNA polymerase inhibitor. Antiviral Res. 100,(2013), 446–454.

[41] Y. Furuta, T. Komeno and T. Nakamura, Favipiravir (T-705), a broad spectrum inhibitor of viral RNA polymerase, Proc. Japan Acad. Ser. B Phys. Biol. Sci. 93(7), (2017) 449–463.

[42] Y. Furuta, K. Takahashi, M. Kuno-Maekawa, H. Sangawa, S. Uehara, K. Kozaki, N. Nomura, H. Egawa, K. Shiraki, Mechanism of action of T-705 against influenza virus. Antimicrob. Agents Chemother. 49, (2005) 981–986.

[43] J. Fischer, C. Ganellin and Robin, Analogue-based Drug Discovery. John Wiley and Sons. (2006).

[44] J. Paeshuyse, K. Dallmeier and J. Neyts, Ribavirin for the treatment of chronic hepatitis C virus infection: a review of the proposed mechanisms of action, Current Opinion in Virology, 1 (6), (2011), 590–598.

[45] Wang, Manli, Ruiyuan Cao, Leike Zhang, Xinglou Yang, Jia Liu, Mingyue Xu, Zhengli Shi, Zhihong Hu, Wu Zhong, Gengfu Xiao, et al. Remdesivir and Chloroquine Effectively Inhibit the Recently Emerged Novel Coronavirus (2019-nCoV) in Vitro, Cell Research 30 (3), (2020), 269–271.

[46] Warren, K. Travis, Robert Jordan, K. Michael, Lo, S. Adrian, Ray, L. Richard, Mackman, Veronica Soloveva, Dustin Siegel, Michel Perron, Roy Bannister, C. Hon, Hui, et al. Therapeutic Efficacy of the Small Molecule GS-5734 against Ebola Virus in Rhesus Monkeys, Nature 531(7594), (2016), 381–85.

[47] Lung, Jrhau, Yu-Shih Lin, Yao-Hsu Yang, Yu-Lun Chou, Li-Hsin Shu, Yu-Ching Cheng, Hung Te Liu, and Ching-Yuan Wu, The Potential Chemical Structure of anti-SARS-CoV-2 RNA-Dependent RNA Polymerase, Journal of Medical Virology, (2020), 1–5.

[48] Chowdhury, Pritom, Marie-Emmanuelle Sahuc, Yves Rouillé, Céline Rivière, Natacha Bonneau, Alexandre Vandeputte, Priscille Brodin et al. Theaflavins, polyphenols of black tea, inhibit entry of hepatitis C virus in cell culture. PloS one 13 (11), (2018), e0198226.

[49] Savarino, Andrea, Livia Di Trani, Isabella Donatelli, Roberto Cauda, and Antonio Cassone, New Insights into the Antiviral Effects of Chloroquine, The Lancet. Infectious Diseases, 6(2), (2006), 67–69.

[50] Yan, Zhen, Yiwu Zou, Yang Sun, Xiao Li, Kai-Feng Xu, Yuquan Wei, Ningyi Jin, and Chengyu Jiang, AntiMalaria Drug Chloroquine is Highly Effective in Treating Avian Influenza a H5N1 Virus Infection in an Animal Model, Cell Research, 23(2), (2013), 300–302.

[51] M.S. Cohen, Hydroxychloroquine for the Prevention of Covid-19 - Searching for Evidence. N. Engl. J. Med. (2020), PMC 7289275.

[52] National Center for Biotechnology Information, Pubchem (Link).

[53] FDA: Emergency Use Authorization Information (Link).